IDŐJÁRÁS

QUARTERLY JOURNAL
OF THE HUNGARIAN METEOROLOGICAL SERVICE

CONTENTS

VOL. 98 * NO. 4 * OCTOBER–DECEMBER 1994

IDŐJÁRÁS

Quarterly Journal of the Hungarian Meteorological Service

Editor-in-Chief
E. MÉSZÁROS

Editor
T. TÄNCZER

Technical Editor
Mrs. M. ANTAL

EDITORIAL BOARD

ANTAL, E. (Budapest)
BOTTENHEIM, J. (Downsview, Ont.)
CZELNAI, R. (Budapest)
DÉVÉNYI, D. (Budapest)
DRĂGHICI, I. (Bucharest)
FARAGÓ, T. (Budapest)
FISHER, B. (London)
GEORGII, H.-W. (Frankfurt a. M.)
GÖTZ, G. (Budapest)
HAMAN, K. (Warsaw)
HASZPRA, L. (Budapest)
IVÁNYI, Z. (Budapest)
KALNAY, E. (Washington, D.C.)
KOLB, H. (Vienna)
KONDRATYEV, K.Ya. (St. Petersburg)
MAJOR, G. (Budapest)
MILOSHEV, G. (Sofia)
MÖLLER, D. (Berlin)
PANCHEV, S. (Sofia)
PRÁGER, T. (Budapest)
PRETEL, J. (Prague)
PRUPPACHER, H.R. (Mainz)
RÁKÓCZI, F. (Budapest)
RENOUX, A. (Paris-Créteil)
ŠAMAJ, F. (Bratislava)
SPÄNKUCH, D. (Potsdam)
STAROSOLSZKY, Ö. (Budapest)
VARGA-HASZONITS, Z. (Budapest)
WILHITE, D.A. (Lincoln, NE)
WIRTH, E. (Budapest)

Editorial Office: P.O. Box 39, H–1675 Budapest

Subscription from customers in Hungary should be sent to the Financial Department of the Hungarian Meteorological Service Kitaibel Pál u. 1, 1024 Budapest. The subscription rate is HUF 2000.

Abroad the journal can be purchased from the distributor: KULTURA, P.O. Box 149, H–1389 Budapest. The annual subscription rate is USD 56.

IDŐJÁRÁS

Quarterly Journal of the Hungarian Meteorological Service
Vol. 98, No. 4, October–December 1994

Recalculation of EMEP photolysis rates as a function of total ozone using LOWTRAN 7 code

D. Bilčík[1], **E. Závodská**[1] and **D. Závodský**[2]

[1] *Geophysical Institute of Slovak Academy of Sciences,*
842 28 Bratislava, Dúbravská cesta 9, Slovakia
[2] *Slovak Hydrometeorological Institute,*
833 15 Bratislava, Jeséniova 17, Slovakia

(Manuscript received 3 May 1994; in final form 18 July 1994)

Abstract—The results of photolysis rates calculation as a function of both the total ozone amount and the solar zenith angle for the EMEP photochemical reactions set are presented. To calculate actinic flux the computer code LOWTRAN 7 was used. The regression expressions were derived to specify the photodissociation rate dependence upon total ozone amount for each of reactions considered.

Key-words: actinic flux, photodissociation rate, total ozone amount.

1. Introduction

Ozone and other photochemical oxidants are natural constituents of the atmosphere. About 90% of the atmospheric ozone is found in the stratosphere. It absorbs most of the solar ultraviolet radiation (UV) before the troposphere is reached. The sources of the tropospheric ozone are influxes from the stratosphere and photochemical production involving nitrogen oxides, hydrocarbons and carbon monoxide from natural and anthropogenic sources.

Up to about 1970 it was thought that photochemical air pollution was concentrated mainly to some urban areas, while the abundance of the tropospheric ozone was predominantly controlled by natural processes. Today is well established that the growing tropospheric ozone level, the most pronounced in middle latitudes of the Northern Hemisphere, results from the increasing emissions of the anthropogenic ozone precursors (*Bojkov,* 1993).

Elevated ozone concentrations are produced by a complex series of the photo and thermal chemical reactions. The representation of these complex reactions is not straightforward in chemical computer models because of the widespread spatial distribution of the precursors and because of the many hundreds of chemical species and reactions believed to be involved. Nevertheless, despite of their apparent complexity, the computer models appear to offer the only approach to gaining the necessary understanding of the ozone creation process and to accepting a national ozone control strategy.

Perturbations to stratospheric O_3 and resulting increase of the UV solar radiation also significantly influence the rates of the key tropospheric photochemical processes. It is believed that feedbacks resulting from the future ozone layer depletion will intensify the tropospheric photochemistry (*Thompson*, 1992; *Závodský* and *Závodská*, 1992). This effect should also be taken into account by formulation of ozone control strategy.

Tropospheric chemistry model simulations often apply the photodissociation rates which are calculated for the typical summer total ozone amount (350 DU). This paper brings the results of photolysis rates calculation as a function of the both total ozone amount and the solar zenith angle for the EMEP photochemical reactions set (*Simpson*, 1992, 1993).

2. Photochemistry in EMEP model

The Meteorological Synthesizing Centre-West of the Co-operative Programme for Monitoring and Evaluation of the Long-range Transmission of Air Pollutants in Europe (EMEP) have developed an ozone model capable of addressing both the problem of short-term episodic ozone and long-term (growing season) ozone (*Simpson*, 1992, 1993). The chemical scheme of this model is updated version of the old EMEP model (*Eliassen et al.*, 1982; *Hov*, 1987). The full scheme of the model includes 45 chemical species, about 100 thermal and 16 photochemical reactions (*Table 1*).

The results of comparison of 25 chemical mechanisms from various photochemical models were recently published (*Derwent*, 1990, 1993). An evaluation of the EMEP chemical mechanism has revealed that it generates the results for ozone, peroxyacetylnitrate and hydrogen peroxide which lie within the central range expected if any of 25 chemical mechanisms had been implemented.

Photodissociation rates of 16 photochemical reactions in EMEP model are the same as those used in the Harwell photochemical model (*Hough*, 1986, 1988). In this work we used the atmospheric transmission and radiance model LOWTRAN 7 (ONCORE, 1991) to recalculate the Harwell photolysis rates. This computer code more realistic considers the important physical processes in cloudless aerosol atmosphere that control the transfer of solar radiation.

Table 1. Photolytic reactions of the EMEP model

Reaction No.	Process	Effective wavelength region
1	$O_3 \rightarrow O_2 + O(^1D)$	290–320 nm
2	$O_3 \rightarrow O_2 + O(^3P)$	290–660 nm
3	$NO_2 \rightarrow NO + O(^3P)$	290–420 nm
4	$NO_3 \rightarrow NO + O_2$	585–635 nm
5	$NO_3 \rightarrow NO_2 + O(^3P)$	400–635 nm
6	$N_2O_5 \rightarrow NO_2 + NO_3$	290–360 nm
7	$HNO_3 \rightarrow NO_2 + OH$	290–330 nm
8	$HCHO \rightarrow HCO + H$	290–335 nm
9	$HCHO \rightarrow H_2 + CO$	290–360 nm
10	$H_2O_2 \rightarrow 2OH$	290–370 nm
11	$CH_3OOH \rightarrow CH_3O + OH$	290–350 nm
12	$CH_3CHO \rightarrow CH_3 + CO + H$	290–340 nm
13	$HCOCHO \rightarrow HCHO + H_2 + CO$	290–470 nm
14	$CH_3COCHO \rightarrow CH_3CO + CO + H$	290–470 nm
15	$CH_3COCOCH_3 \rightarrow CH_3CO + CH_3CO$	290–470 nm
16	$C_2H_5COCH_3 \rightarrow C_2H_5 + CH_3CO$	290–335 nm

3. *Photolysis rates calculation*

3.1 Theoretical assumptions

For each photoactive molecule the photodissociation rate coefficient J is calculated by integrating over the effective wavelength interval (λ_1, λ_2) the product of the spectral actinic flux F_A (λ), the spectral absorption cross section σ (λ), and the photodissociation quantum yield φ (λ) (*Madronich*, 1987):

$$J = \int_{\lambda_1}^{\lambda_2} \varphi(\lambda)\, \sigma(\lambda)\, F_A(\lambda)\, d\lambda \,. \tag{1}$$

The actinic flux F_A (λ) is defined as the spherically integrated solar photon flux incident onto an infinitesimal volume element in the atmosphere. F_A (λ) must be in units of photons per unit area per unit time per unit wavelength interval. It depends on many factors: ozone and molecular oxygen absorption, aerosol absorption, molecular (Rayleigh) and aerosol (Mie) scattering, Earth's surface reflection.

The actinic flux F_A (λ) may be split into a direct and a diffuse part:

$$F_A(\lambda) = F_0(\lambda) + F\downarrow(\lambda) + F\uparrow(\lambda). \tag{2}$$

The first component $F_0(\lambda)$ is the directly transmitted solar irradiance, while the rest two components $F\downarrow(\lambda)$ and $F\uparrow(\lambda)$ represent the downward and the upward diffuse contributions. Whereas the direct component $F_0(\lambda)$ can be calculated using a simple exponential formula, the diffuse components require angular integration over hemisphere:

$$F\downarrow(\lambda) = \int_0^{2\pi}\int_0^{1} L\downarrow(\lambda,\mu,\varphi)\, d\mu\, d\varphi, \tag{3}$$

$$F\uparrow(\lambda) = \int_0^{2\pi}\int_{-1}^{0} L\uparrow(\lambda,\mu,\varphi)\, d\mu\, d\varphi, \tag{4}$$

where μ and φ are the cosine of zenith angle and the azimuthal angle, respectively. Even if angular distribution of both the downward $L\downarrow$ and the upward $L\uparrow$ radiance is known, the calculation is too much time consuming from practical applications point of view. Therefore appropriate approximations of angular integrals in Eqs. (3) and (4) are useful. The most common approximation used in the radiation model calculations for the upward radiance is an asumption of isotropic surface reflection (Lambertian surface), i.e. $L\uparrow(\mu,\varphi)$ = constant. In this case the upward component of the actinic flux can be calculated as (*Madronich*, 1987)

$$F\uparrow(\lambda) = A(2\mu_0 F_0(\lambda) + F\downarrow(\lambda)), \tag{5}$$

where A is the surface albedo and μ_0 is cosine of solar zenith angle.

The downward radiance $L\downarrow$ in the atmosphere with aerosol particles is highly anisotropic. However, according to *Ruggaber et al.* (1993) for the diffuse part of the actinic flux only the azimuthally independent radiance is relevant. Therefore the azimuthally dependent radiance in Eq. (3) can be replaced either by its mean value or by a value at a fixed azimuth angle φ_r, which represents approximately the mean radiance. To avoid the integration over all zenith angles in Eq. (3) a similar approximation is necessary, i.e. to use the irradiance value at a fixed zenith angle $\theta_r = \cos^{-1}\mu_r$, which corresponds to mean radiance (*Madronich*, 1987). We can then write for downward diffuse part of the actinic flux:

$$F\downarrow(\lambda) = 2\pi L\downarrow(\lambda,\theta_r,\varphi_r). \tag{6}$$

θ_r and φ_r are the zenith angle and the relative azimuth (to the Sun position),

respectively. The angle of 1 radian for θ_r (*Hough*, 1988) and the same value for a relative azimuth φ_r was used in our calculation. *Figs. 1a, b* illustrate the comparison of downward radiance values calculated at a reference point (φ_r = 1 rad, θ_r = 1 rad) with azimuthally averaged values calculated using 20 points Gaussian quadrature for the azimuth integral. It can be seen that in UV region the differences are negligible. At the longer wavelenghts ($\lambda > 400$ nm) these differences are small and depend upon the Sun position.

Using above mentioned approximations with combination of Eqs. (2) and (5) we can determine the actinic flux as

$$F_A(\lambda) = F_0(\lambda)(1 + 2A\mu_0) + F\downarrow(\lambda)(1 + A). \tag{7}$$

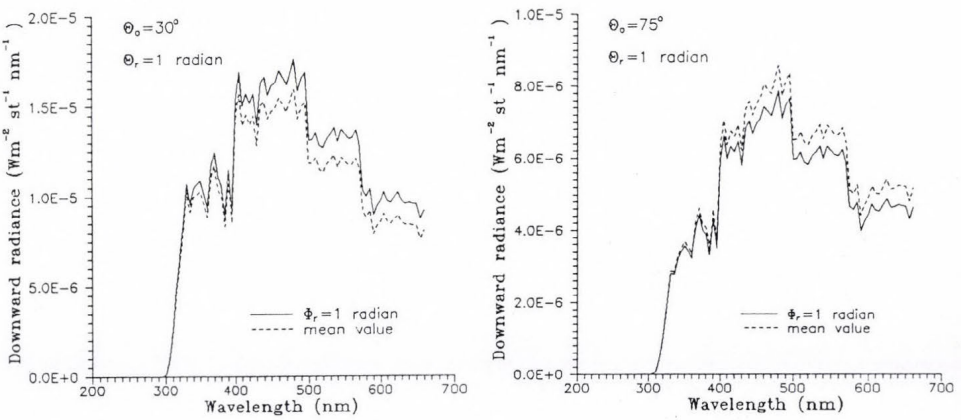

Fig. 1. Comparison of downward radiance values calculated for θ_r and φ_r (1 rad) with azimuthally averaged values; solar zenith angle (*a*) $\theta_0 = 30°$, (*b*) $\theta_0 = 75°$.

3.2 Radiative transfer model and input data

The computer code LOWTRAN 7 was utilized to calculate the directly transmitted solar irradiance and the path radiance ($L\downarrow$ in Eqs. (3) and (6)) in the inhomogeneous aerosol cloudless atmosphere with spectral resolution of 50 cm^{-1}. In addition to Rayleigh scattering and molecular absorption this code includes the aerosol extinction. The contributions of multiple scattered photons to the total path radiance are also included. Scattering caused by air molecules and aerosol particles is treated separately using different phase functions. The Mie generated phase functions corresponding to the different aerosol models are used for aerosol scattering.

The model atmosphere is composed of 31 homogeneous plane-parallel layers of unequal thickness. The top of the atmosphere is situated at 50 km hight.

Table 1 contains the list of 16 photochemical reactions with the effective wavelength intervals for which the calculations have been made. To calculate the photolysis rates of the reaction i Eq. (1) can be evaluated by summation over finite wavelength intervals:

$$J_i = \sum_{n=1}^{N_i} \varphi_{i,n} \sigma_{i,n} F_{A,n}, \tag{8}$$

where N_i is the total number of 5-nm intervals covering the effective wavelength region of reaction i (see Table 1). All values of φ_n, σ_n for each photochemical reaction are taken from *Hough* (1988). $F_{A,n}$ represent the integrated values of the actinic flux over individual 5-nm intervals.

The actinic flux was calculated at 0.5 km level for five total ozone amounts (200, 250, 300, 350, and 400 DU) and for five Sun positions. Although the relation Eq. (5) is valid only for a level close to the Earth's surface, we used it at level of 0.5 km, because the contribution of layer below the 0.5 km level to the upwelling diffuse radiation is small compared to the total downwelling radiation.

Vertical ozone profiles follow the Mid-Latitude Summer profile (*Ellingson et al.*, 1991). We considered a Lambertian surface with albedo of 0.10. We used the LOWTRAN 7 boundary layer (0–2 km) rural (visibility of 23 km) and stratospheric background aerosol models.

4. Results and discussion

Figs. 2–17 show the calculated photodissociation rates as a function of both the solar zenith angle and the total ozone column for each of 16 photochemical processes listed in Table 1. All J_i calculations are made at level of 0.5 km above surface with albedo 0.10 (summer conditions). The present results are compared with those of *Hough* (1988) for 350 DU total ozone. Generally, fairly good agreement is found between these two sets of calculation. The differences increase with spreading the effective wavelength region toward the visible part of solar spectrum. In most cases the differences change from positive to negative with increasing solar zenith angle. The dependence of J_i on the solar zenith angle is more intensive in present work. It may be explained by the different method of the radiance calculations. The dependence upon the solar zenith angle may be enhanced due to aerosol particles anisotropic scattering. The solar zenith angle dependence is decreasing with decreasing effective wavelengths, due to an increasing effect of multiple scattering.

Ozone absorption is the dominating process in the wavelength region between 290 and 320 nm (UVB region) and therefore the downward radiance

is less affected by aerosol particles than in other wavelength intervals. This explains why the photolysis rates for ozone photolysis ($O_3 \rightarrow O_2 + O(^1D)$) and HNO_3 photolysis calculated by *Hough* are in excellent agreement with present results (Figs. 2 and 8).

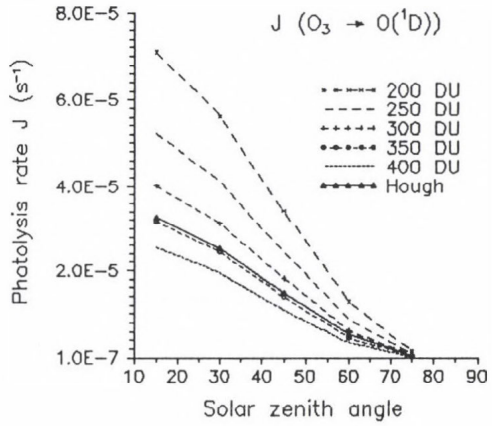

Fig. 2. The calculated photolysis rate $J(O_3 \rightarrow O(^1D))$ as a function of solar zenith angle and total ozone amount under clear sky, 0.5 km above surface, 0.10 surface albedo. *Hough* assumed condition clear sky, 0.5 km above land, 350 DU total ozone.

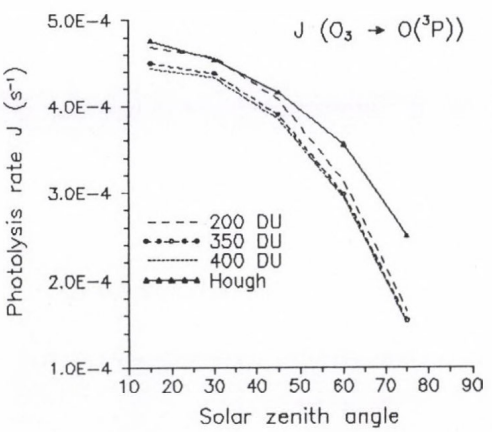

Fig. 3. As Fig. 2, but for $J(O_3 \rightarrow O(^3P))$.

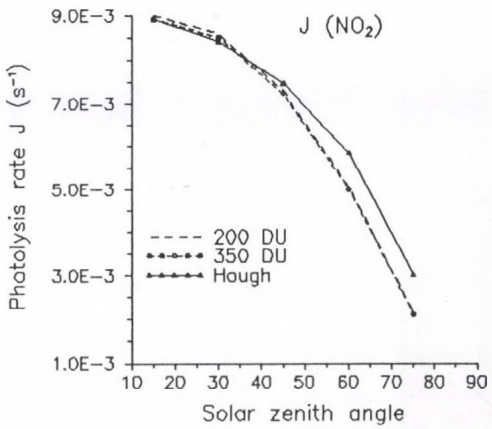

Fig. 4. As Fig. 2, but for $J(NO_2)$.

The effect of variations of the total ozone amount is largest at the photochemical processes with the effective wavelengths in UVB region. The strong ozone absorption in this part of the solar spectrum (Hartley band) results in a strong dependence of the actinic flux as well as the photolysis rates on the total ozone amount (Figs. 2, 7, 8 and 17). The influence of the Chappius band at about 600 nm is smaller (Figs. 5 and 6).

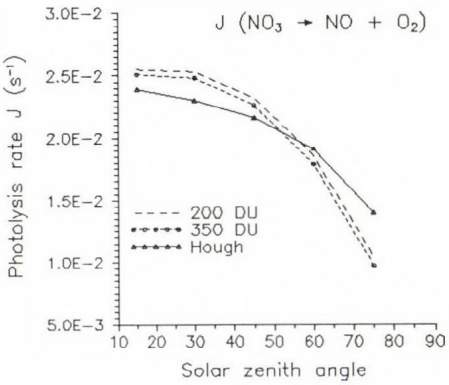

Fig. 5. As Fig. 2, but for $J(NO_3 \rightarrow NO + O_2)$.

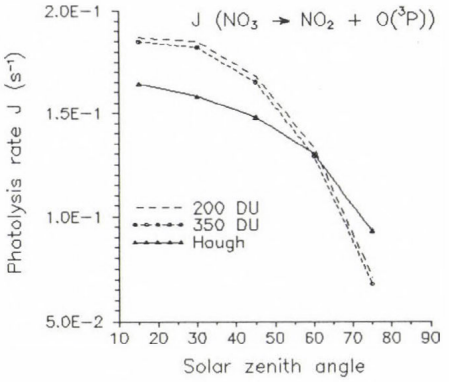

Fig. 6. As Fig. 2, but for $J(NO_3 \rightarrow NO_2 + O(^3P))$.

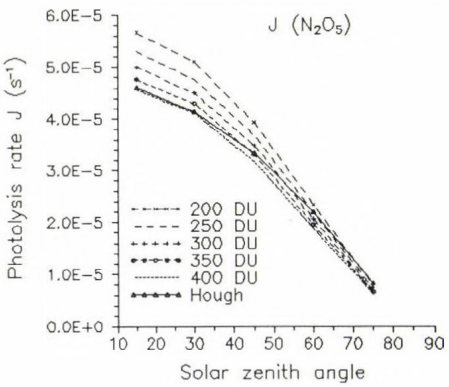

Fig. 7. As Fig. 2, but for $J(N_2O_5)$.

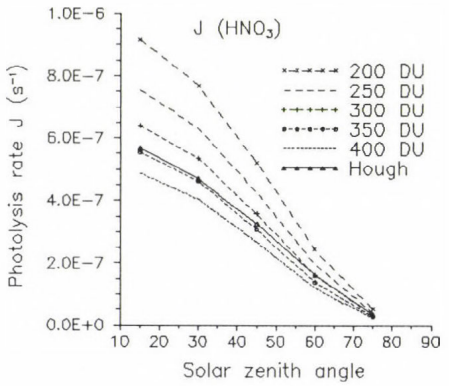

Fig. 8. As Fig. 2, but for $J(HNO_3)$.

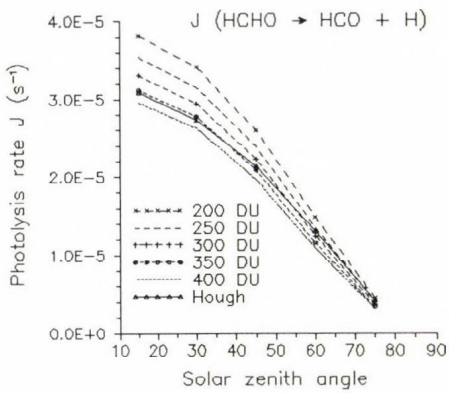

Fig. 9. As Fig. 2, but for $J(HCHO \rightarrow HCO + H)$.

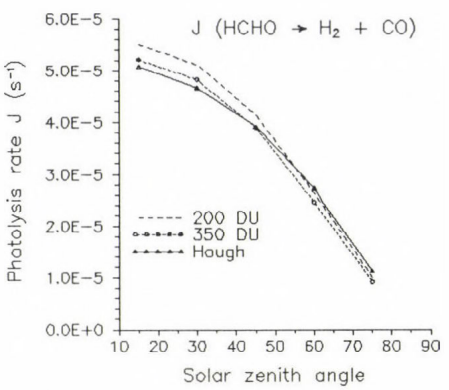

Fig. 10. As Fig. 2, but for $J(HCHO \rightarrow H_2 + CO)$.

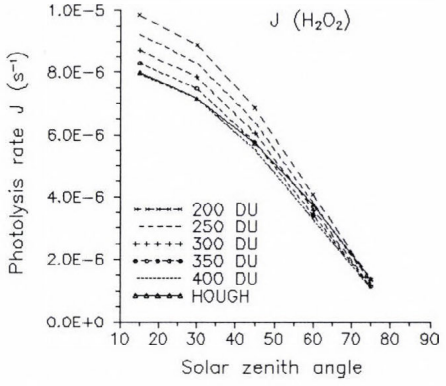

Fig. 11. As Fig. 2, but for $J(H_2O_2)$.

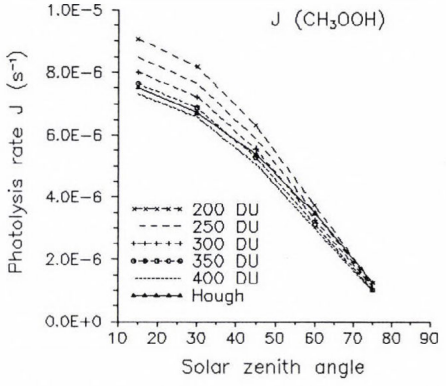

Fig. 12. As Fig. 2, but for $J(CH_3OOH)$.

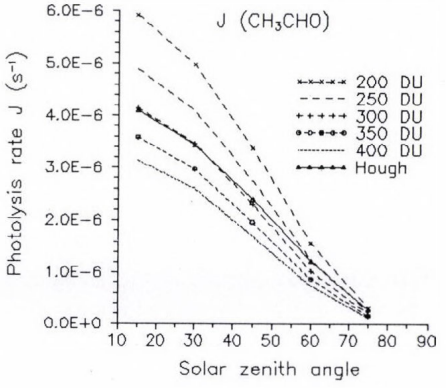

Fig. 13. As Fig. 2, but for $J(CH_3CHO)$.

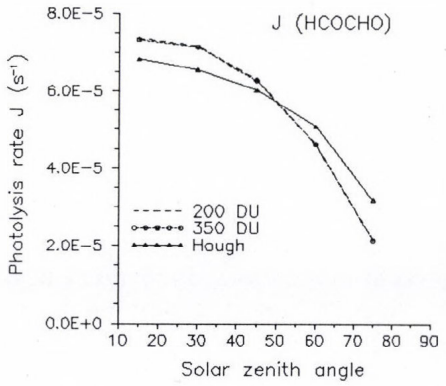

Fig. 14. As Fig. 2, but for J(HCOCHO).

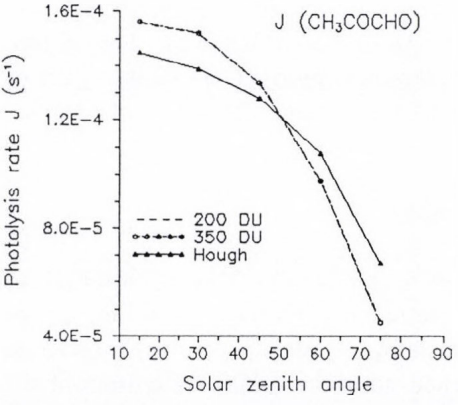

Fig. 15. As Fig. 2, but for $J(CH_3COCHO)$.

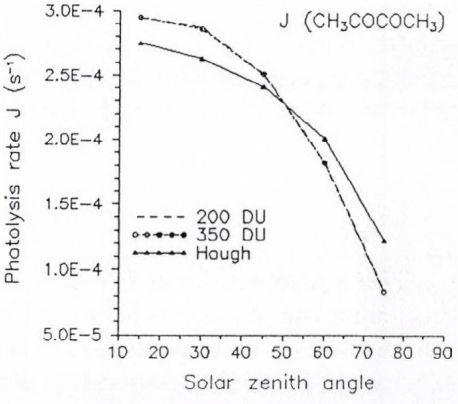

Fig. 16. As Fig. 2, but for $J(CH_3COCOCH_3)$.

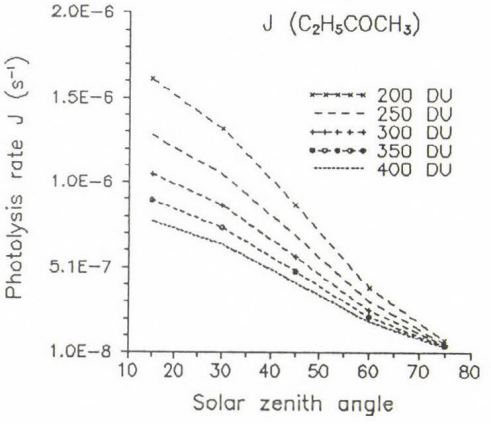

Fig. 17. The calculated photolysis rate $J(C_2H_5COCH_3)$ as a function of solar zenith angle and total ozone amount under clear sky, 0.5 km above surface, 0.10 surface albedo.

For use in tropospheric chemistry model photodissociation rates are specified as a function of both the solar zenith angle (θ_0), and the total ozone column (*Simpson*, 1993):

$$J = a \exp(-b \sec \theta_0). \tag{9}$$

Here a and b are coefficients which for clear sky depend upon the total ozone amount in the atmosphere. In order to indicate this dependence, we used the present photodissociation rate calculations. For the solar zenith angle between 15° and 75° and for the total ozone amount between 200 and 400 DU we derived the exponential expressions for coefficients a and b:

$$a = A_a \exp(B_a x), \quad b = A_b \exp(B_b x), \tag{10}$$

where x is the total ozone amount in DU. *Table 2* presents the regression coefficients A_a, B_a, A_b and B_b for each of reactions considered. The photochemical processes with the effective wavelength region in the visible part of solar spectrum are practically independent of total ozone amount.

5. *Conclusions*

The transmission and radiance model LOWTRAN 7 were applied to recalculate the photolysis rates of 16 photochemical reactions used in long-range transport air pollution models. The regression expressions were derived to specify the photodissociation rate dependence upon the total ozone amount for each of reactions considered. The calculations were made for the level of 0.5 km above surface with the albedo of 0.10. The calculated data were compared

with those used in EMEP model for 350 DU total ozone. Generally good agreement but some differences were found. These may be explained by the different method of the actinic flux calculation.

Table 2. Regression coefficient values in relations (10)

Reaction No.	Regression coefficient			
	A_a	B_a	A_b	B_b
1	5.108E-4	-3.937E-3	1.129E+0	8.245E-4
2	7.182E-4	-2.184E-4	3.642E-1	1.270E-4
3	1.516E-2	-4.895E-5	5.115E-1	+
4	3.654E-2	-2.576E-5	3.086E-1	2.980E-4
5	2.717E-1	*	3.572E-1	*
6	7.791E-5	-1.059E-3	1.518E+0	2.356E-5
7	4.024E-6	-2.940E-3	9.603E-1	2.421E-4
8	9.510E-5	-1.090E-3	7.106E-1	2.636E-4
9	1.040E-4	-2.876E-4	5.885E-1	1.246E-4
10	2.307E-5	-1.063E-3	6.952E-1	+
11	2.127E-5	-1.044E-3	7.021E-1	+
12	2.501E-5	-2.603E-3	9.258E-1	5.228E-4
13	1.165E-4	*	4.427E-1	*
14	2.487E-4	*	4.461E-1	*
15	4.722E-4	*	4.538E-1	*
16	8.275E-6	-3.704E-3	1.030E+0	+

* in this case a and b are independent of total ozone amount ($a = A_a$, $b = A_b$)
\+ in this case b is independent of total ozone amount ($b = A_b$) coefficients A_a are in s^{-1}

References

Bojkov, R.D., 1993: Changes in ozone distribution: European aspects. *Extended Abstracts, WMO Region VI Conference on the Measurement and Modelling of Atmospheric Composition Changes Including Pollution Transport.* 4-8 October, Sofia, Bulgaria, 13-16.

Derwent, R.G., 1990: Evaluation of photochemical mechanisms for their application in models describing the formation of photochemical ozone in Europe. *Atmos. Environ. 24A*, 2615-2624.

Derwent, R.G., 1993: Evaluation of the chemical mechanism employed in the EMEP photochemical oxidant model. *Atmos. Environ. 27A*, 277-279.

Eliassen, A., Hov, O., Isaksen, I.S.A., Saltbones, J. and *Stordal, F.*, 1982: A Lagrangian long-range transport model with atmospheric boundary layer chemistry. *J. Appl. Meteor. 21*, 1645-1661.

Ellingson, R.G., Ellis, J. and *Fels, S.*, 1991: The intercomparison of radiation codes used in climate models: Long-wave results. *J. Geophys. Res. 96*, 8929-8953.

Hough, A.M., 1986: The production of photochemical pollution in Southern England and the effects of vehicle exhaust emis-

sion control strategies. Harwell Laboratory. *Report* AERE R 12069.

Hough, A.M., 1988: The calculation of photolysis rates for use in global tropospheric modelling studies. Harwell Laboratory. *Report* AERE R 13259.

Hov, O., 1987: Models for photochemical processes. In *Regional and Long-range Transport of Air Pollution*. Elsevier, Amsterdam, pp. 391-412.

Madronich, S., 1987: Photodissociation in the atmosphere. 1. Actinic flux and the effects of ground reflections and clouds. *J. Geophys. Res. 92*, 9740-9752.

ONCORE, 1991: *Personal Computer Version of the LOWTRAN 7 Atmospheric Model, Version 2a*. Ontar Corporation.

Ruggaber, A., Forkel, R. and *Dlugi, R.*, 1993: Spectral actinic flux and its ratio to spectral irradiance by radiation transfer calculations. *J. Geophys. Res. 98*, 1151-1162.

Simpson, D., 1992: Long-period modelling of photochemical oxidants in Europe. Model calculations for July 1985. *Atmos. Environ. 26A*, 1609-1634.

Simpson, D., 1993: Photochemical model calculations over Europe for two extended summer periods: 1985 and 1989. *Atmos. Environ. 27A*, 921-943.

Thompson, A.M., 1992: The oxidizing capacity of the Earth's atmosphere: Probable past and future changes. *Science 256*, 1157-1165.

Závodský, D. and *Závodská, E.*, 1992: Air quality and climate change (in Slovak). In *National Climate Programme CSFR No. 7*, CHMI, Prague, pp. 3-52.

IDŐJÁRÁS

Quarterly Journal of the Hungarian Meteorological Service
Vol. 98, No. 4, October–December 1994

Temperature variation in Europe and North America since the beginning of instrumental observations

G. Koppány

Department of Climatology, József Attila University,
H-6722 Szeged, P.O. Box 661, Hungary

(Manuscript received 22 June 1994; in final form 20 November 1994)

Abstract—With the intention of analysis, 19 climatological stations were selected possessing annual mean temperature series longer than 150 years. The running 9-year mean temperatures were used in order to determine the coincidences of simultaneous warmings and coolings at different places in central, western and northern Europe, as well as in the eastern U.S.A. Several short periods were found with simultaneous maxima or minima at many different locations. Comparing these periods with volcanic activity,it is pointed out that the temperature minima are close to high volcanic activities, and maxima to calm volcanic episodes. It were also found that in 9 stations out of 19, temperature maxima before 188O were higher than those after 188O. It is likely that the global mean temperature had relatively low value around 188O.

Key words: long-term temperature variations, volcanic activity.

1. Introduction

It is widely known that the global near surface temperature has increased by cca 0.5°C since the 1880-s (*Götz*, 1983; *Lockwood*, 1986; *Brazdil et al.*, 1987). The warming was as much as 0.8°C in the Northern Hemisphere, and reached its maximum in years 1938–1940. Many authors concluded that this warming is the response of the atmosphere to increasing CO_2 after beginning of industrialisation and technical development from late 19-th century (*Energy and Climate*, 1977). Moreover, according to numerical climate model experiments the global warming may reach 2–5°C by 21-st century, if the increase of atmospheric CO_2 will continue with present rate (*Bach* and *Jain*, 1991; *Houghton*, 1994). This warming may result in shifts of climatic zones.

However, the question is, whether the temperature variations could be explained by means of a single factor, namely the change of atmospheric CO_2

and other greenhouse-gases (CH_4, N_2O etc.). It is also well known that the energy flux density of anthropogeneous sources in area as large as several 100 km (megapolises, industrial centres) approaches the net solar radiation density, which is about 100 W/m^2 (*Lockwood*, 1986; *Koppány*, 1989). On the other hand, many climatic stations are located in areas with dense population. Thus, at least a fraction of the global warming is apparent and may be the consequence of urbanization.

It is also noteworthy that the global mean temperature decreased by around 0.3°C from 1940 to 1979, while cooling in the Northern Hemisphere was as much as 0.5°C. This fact suggests that the atmospheric temperature is influenced by other factors besides the greenhouse effect since the atmospheric carbon-dioxide has grown after 1940 continuously.

Therefore it is reasonable to investigate temperature series of length more than 150 year in order to decide: whether significant warming took place before 1880, too, and if yes, then these pre-industrial warmings were higher or lower, than those in the 20-th century. 19 climatic stations were selected possessing more or less continuous temperature series from early 19-th century or further back. The records available from these stations are insufficient for calculation mean global or hemispheric temperature variations. Still the early instrumental measurements might provide some information on regional temperature changes occured in last 2 or 3 centuries mainly from great part ot Europe, and from eastern United States.

2. Data sources

The temperature records have been taken mostly from Bracknell data basis up to 1960 in form of magnetic tapes. Some additional series were obtained from *Ch. D. Schönwiese*, Goethe University of Frankfurt am Main, among others the records of Central England (*Schönwiese*, 1988), and the data period 1961-70 from *World Weather Records* (1971). The series of Budapest since 1780 are available in *A. Réthly*'s work (*Réthly*, 1947), and in file of the Hungarian Meteorological Service. The list of climatic stations is presented in *Table 1*.

The majority of stations (14) is located between 46–56°N latitudes, i.e. in temperate zone, three stations are in subtropical zone, and two stations in subpolar zone, respectively. 16 stations have continuous temperature series, two stations have interrupted series (Charleston and Copenhagen), in these cases either only the continuous part was used or the short interruptions were completed by interpolation. The records of Prague from 1939 to 1950 were added to those obtained from Bracknell.

Table 1. Geographical positions and observation periods of climatic stations

Station	Latitude	Longitude	Observation period(s)
Central England	52.8°N	2.5°W	1659–1987
De Bilt	52.6°N	5.1°E	1706–1970
Charleston (U.S.A.)	32.9°N	80.0°W	1741–1759, 1823–1965
Edinburgh	55.9°N	3.2°W	1764–1970
Basel	47.6°N	7.6°E	1755–1970
Geneva	46.2°N	6.2°E	1753–1970
Trondheim	63.4°N	10.4°E	1761–1969
Stockholm	59.4°N	18.0°E	1757–1970
Copenhagen	55.6°N	12.5°E	1768–1776, 1782–1788, 1798–1970
Greenwich	51.5°N	0.0°	1763–1970
Berlin	52.6°N	13.4°E	1769–1970
Paris	48.8°N	2.5°E	1764–1970
Prague	50.1°N	14.4°E	1771–1989
New Haven (U.S.A.)	41.3°N	72.9°W	1781–1970
Hohenpeissenberg	47.8°N	11.0°E	1781–1970
Vienna	48.3°N	16.4°E	1775–1970
Budapest	47.5°N	19.0°E	1780–1970
Kremsmünster	48.1°N	14.1°E	1796–1985
Genova	44.5°N	3.5°E	1833–1986

3. Method and results

As a first step decadal mean temperatures were calculated for all available climatic stations. By analyzing such rough materials synchronous warmings or coolings appeared in some stations, e.g. the decade of *1731–1740* proved warm both in Central England and De Bilt with positive decadal temperature anomaly (+ 0.4°C). Similar relative *warming* occured in *1791–1800* at twelve stations, in *1861–1870* at eleven stations etc. On the other hand, relatively great negative anomalies were found in *1811–1820* at eight stations, in *1881–1890* at 13 climatic stations etc.

In order to get more exact periods of local warming and cooling at various stations, running 9-year averages were determined. The standard deviations of 9-year mean temperatures and the mean values of the whole series were also calculated for each station. The secular temperature variations are presented in *Fig. 1 a-f.* The arrows directing upwards denote warming, 'M' marks the maxi-

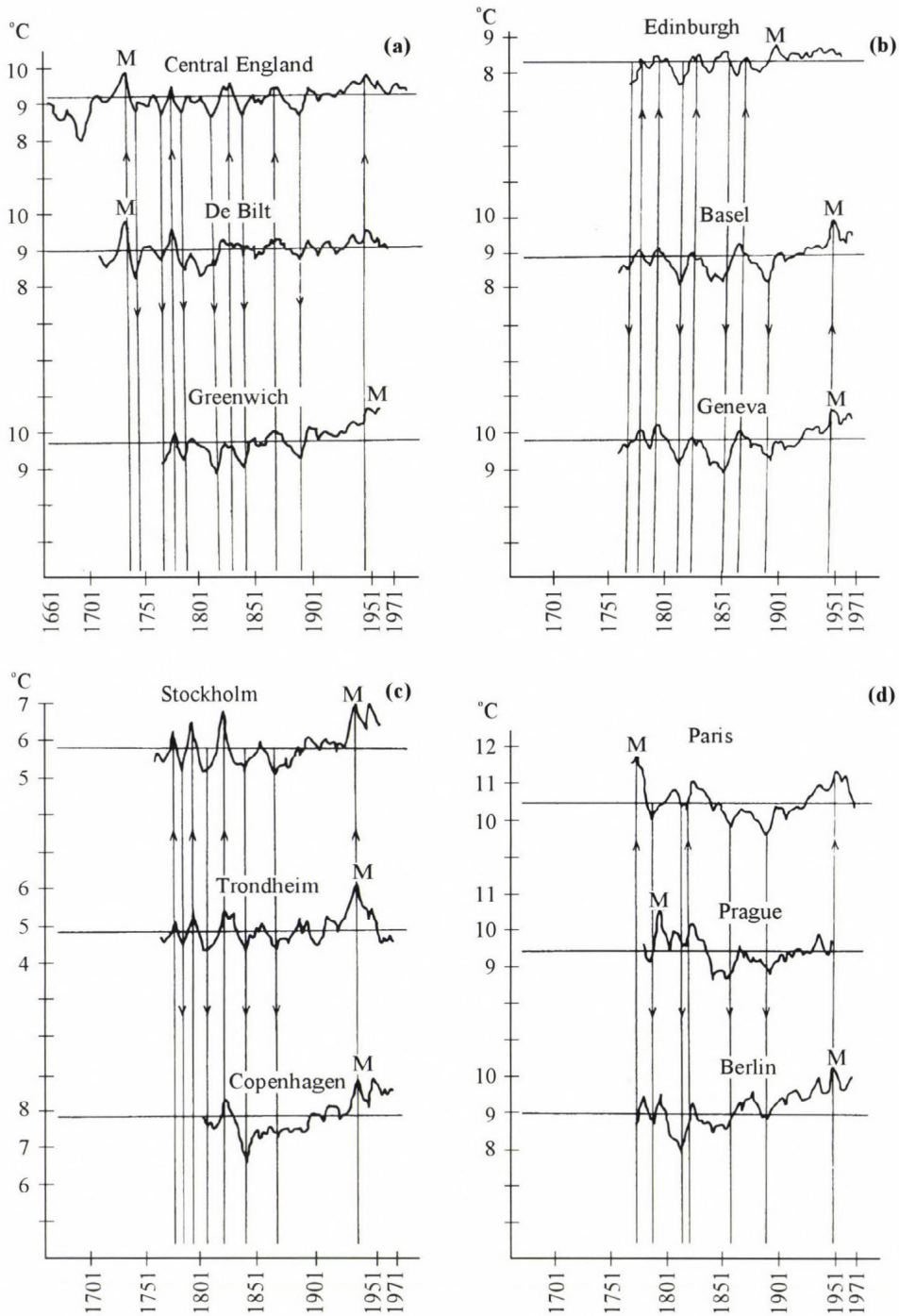
°C
(a)
Central England
De Bilt
Greenwich
M
10
9
8
1661
1701
1751
1801
1851
1901
1951
1971
(b)
Edinburgh
Basel
Geneva
(c)
Stockholm
Trondheim
Copenhagen
(d)
Paris
Prague
Berlin

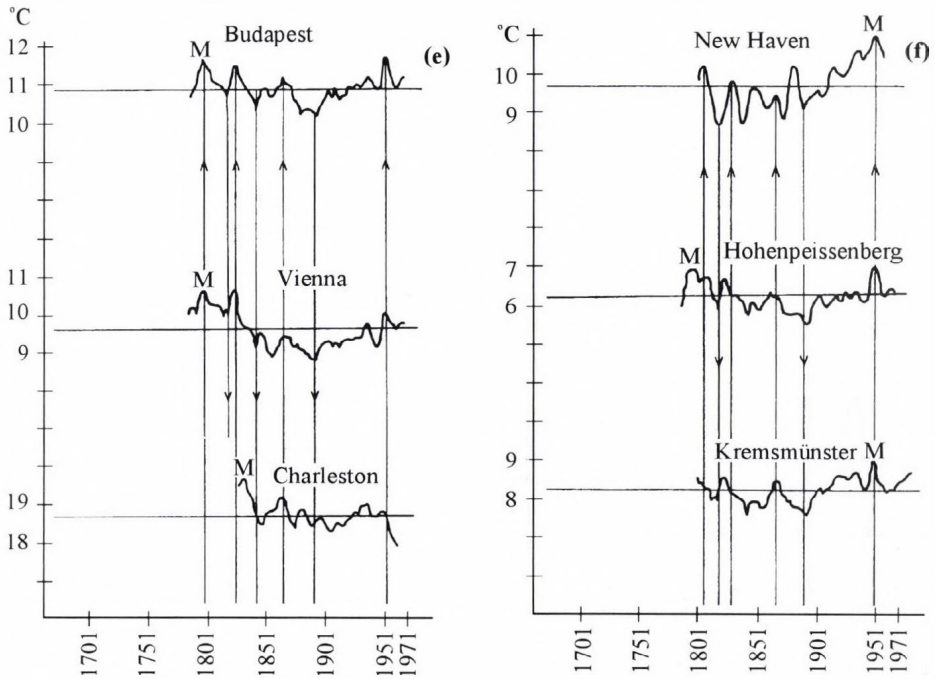

Fig. 1a-f. Running 9-year mean temperature since beginning of instrumental observation at different station.

mum value in whole series of a given station, the arrows directing downwards denote cooling. One can recognize *synchronous maxima* in some stations in periods of 1772–1779, of 1790–1794, of 1822–1830, of 1859–1865, of 1893-1897, of 1930-s and 1940-s. On the other hand, *minima* can be found in some stations in periods of 1767–1770, of 1812–1816, of 1836–1841, of 1888–1891, of 1903–1905 and 1960-s.

Schönwiese (1988) has found significant negative correlation between the mean temperature of Northern Hemisphere and several kinds of volcanic indices. In *Fig. 2* the spells of synchronous warmings and coolings are presented during the period of 1731–1970 (above), while the dust vail index (DVI) is shown below since 1750, with the names of greater volcanic eruptions. According to the DVI data the calm volcanic periods were: (1) 1770–1780, (2) 1790–1810, (3) 1820–1831, (4) 1845–1880 and (5) 1913–1962. These calm periods coincided with the years of temperature maxima mentioned above. Unusually long *volcanic* silence appeared between 1912 and 1963, which coincided with the significant warming in the 20-th century. On the other hand

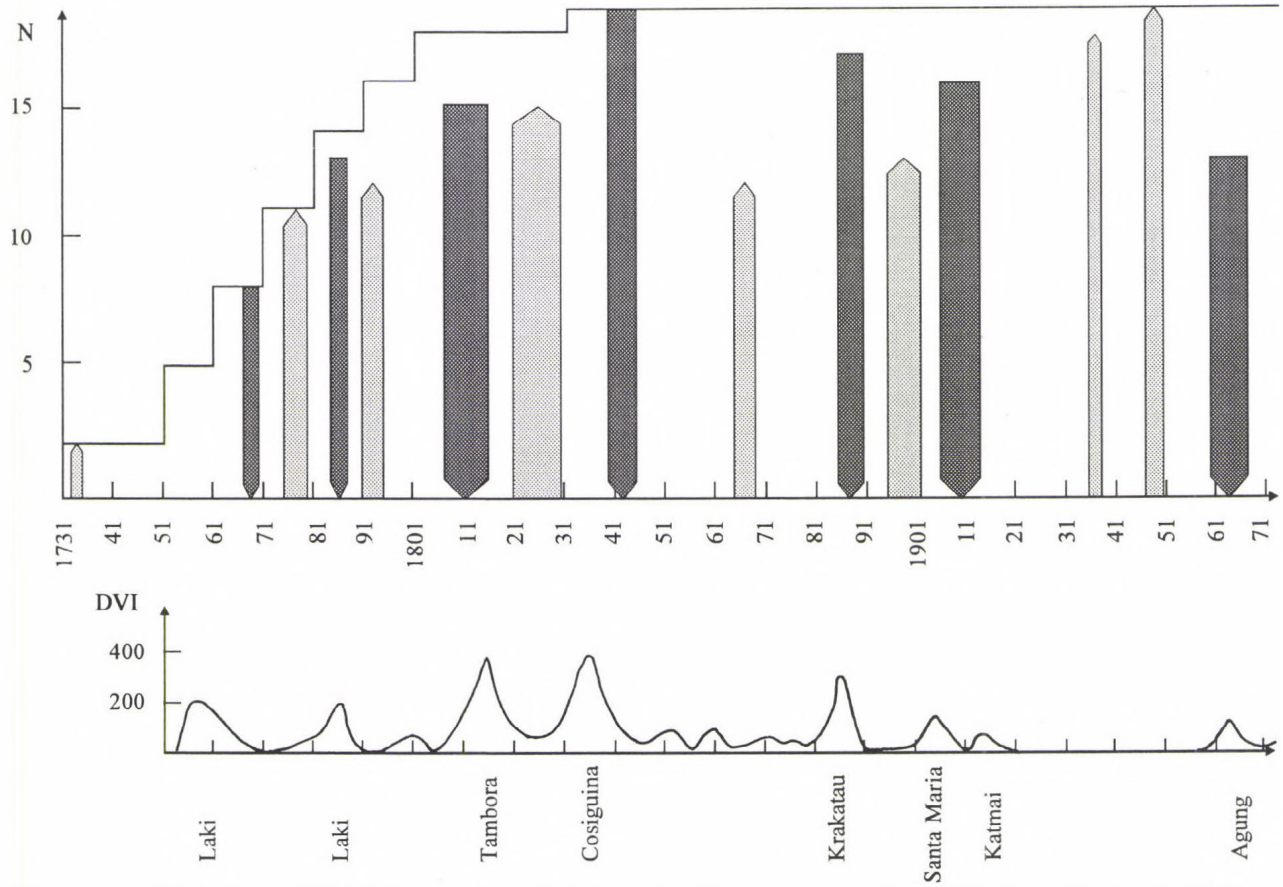

Fig. 2. Above: Number of climatic stations (N) possessing data since 1731; arrows upwards denote the number of stations with synchronous maxima, downwards denote the number of stations with simultaneous minima. The widths of the arrows indicate the lengths of spells with synchronous extreme temperature. *Below*: dust veil index with the names of greater volcanic eruptions.

several strong volcanic eruption occured since 1756 over the period included in this investigation (e.g. Laki, Iceland in 1756 and 1785; Tambora between 1815 and 1822; Krakatau in 1875–83; Santa Maria, Mount Pelee, and Colima in 1902; Katmai, Alaska in 1912; Agung, Bali 1963). The coincidences of active volcanic spells with cooling in the majority of climatic stations are evident in Fig. 2. Besides the direct insolation has weakened by around 5 per cent after 1950 due to *increasing atmospheric turbidity* as a probable consequence of increased aerosol emitted by human activity (*Pivovarova*, 1970; *Budyko*, 1982; *Budyko et al.*, 1987). A similar cooling effect was pointed out by *Houghton* (1994).

One of the main purpose of this study is to investigate the temperature maxima *before 1880* and to reveal the evidence of warmer periods comparing with those in the *20-th century*. *Table 2* contains the highest running 9-year mean temperature anomalies at each station, before and after *1880*. In the first column one can find the mean temperature for the whole series, and in the second column the standard deviation of running 9-year averages (s). The next column presents the maxima years and the temperature anomalies in form of the ratio k = anomaly per standard deviation i.e. signal per noise, both concerning the warmings before *1880*. The next column contains the same characteristics but after *1880*, while in last column *dt* denotes the difference between the maximum annual temperature in 20-th century and the maximum annual temperature before 1880. If the difference is positive that means relative warming in the 20-th century, if it is negative, the stronger warming took place before 1880. The latter cases are marked with exclamation point. Nine stations out of 19 have proved relative greater warming before 1880, among others Charleston and Prague, Paris, Vienna, De Bilt, Genova etc.

Hence it seems, that there were significant warmings in the both 18-th and the 19-th century, i.e. before the significant increase of atmoshperic carbon-dioxide started due to industrialization. *Keil* (1961), analyzing long temperature series of Basel, Hohenpeissenburg, Jena and Prague, has got similar results using 30–40–50–60-year smoothed temperature data.

After maxima in the 1930-s or the 1940-s an overall cooling was observed during the 1950-s or the 1960-s in all stations (*Table 3*). The ratio k = (difference between maximum and minimum per standard deviation) exceeds 1 at 16 stations, 2 at 7 stations and 3 at 2 stations.

4. Conclusions

— The temperature series over a period longer than 150 years exhibit minima between 1886 and 1891 at the majority of the climatic stations (see Fig. 2).
— Temperature maxima occured many times before 1880, and at 45

percent of the stations these maxima were higher, than those in 1930-s and 1940-s.

— The warming in the 1930-s or the 1940-s coincides with the longest calm volcanic period since 1750.
— A uniform cooling took place by the 1950-s or the 1960-s.
— In the light of these facts the global temperature variations may not be explained exclusively with greenhouse effect.

Table 2. The warmest running 9-year mean temperature

Station	°C	s °C	Before 1880 (k)		After 1880 (k)		dt °C
Basel	8.9	0.38	1794	+0.87	1947	+2.95	+0.67
			1865	+1.18			
Berlin	8.9	0.36	1794	+1.44	1947	+1.28	- 0.50 !
			1876	+1.69			
Budapest	10.9	0.33	1794	+2.52	1949	+2.45	- 0.20 !
Charleston	18.7	0.35	1831	+2.86	1935	+0.94	- 0.70 !
New Haven	9.7	0.59	1790	+1.57	1949	+2.19	+0.73
Central England	9.2	0.33	1734	+2.36	1947	+2.00	- 0.12 !
			1830	+1.33			
Copenhagen	7.8	0.49	1922	+1.04	1947	+2.20	+0.57
De Bilt	9.0	0.33	1733	+2.87	1947	+2.10	- 0.23 !
			1777	+2.03			
Edinburgh	8.3	0.26	1794	+0.65	1936	+1.65	+0.12
			1854	+1.19			
Geneva	9.8	0.38	1794	+1.32	1947	+2.53	+0.46
Genova	15.7	0.36	1865	+2.50	1946	+1.67	- 0.30 !
Greenwich	9.7	0.39	1779	+0.69	1947	+2.38	+0.66
Hohenpeissenberg	6.2	0.33	1794	+2.39	1949	+2.45	+0.02
Kremsmünster	8.2	0.31	1800	+1.13	1947	+2.45	+0.41
Paris	10.5	0.46	1772	+2.67	1949	+1.76	- 0.42 !
Prague	9.5	0.52	1793	+2.11	1949	+1.35	- 0.40 !
Stockholm	5.8	0.48	1794	+1.48	1947	+2.67	+0.28
			1822	+2.08			
Trondheim	4.8	0.37	1794	+1.43	1934	+3.38	+0.70
			1822	+1.49			
Vienna	9.6	0.50	1798	+2.18	1949	+1.04	- 0.57 !

Table 3. Maxima and subsequent minima (years and values) of 9-yr running averages of temperature in the 20th century and the magnitude of the cooling after 1930s or 1940s; *k* is the difference between maximum and minimum per standard deviation

Station	Year	°C	Year	°C	°C	k
Central England	1947	9.8	1966	9.2	-0.6	-1.91
De Bilt	1947	9.6	1966	8.9	-0.7	-2.37
Greenwich	1947	10.7	1954	10.5	-0.2	-0.51
Edinburgh	1936	8.8	1954	8.4	-0.4	-1.23
Basel	1947	10.0	1959	9.3	-0.7	-1.79
Geneva	1947	10.7	1954	10.2	-0.5	-1.26
Stockholm	1947	7.1	1954	6.3	-0.8	-1.56
Trondheim	1934	6.1	1954	4.4	-1.7	-4.49
Copenhagen	1947	8.9	1966	8.3	-0.6	-1.14
Paris	1949	11.3	1966	10.2	-1.1	-2.37
Prague	1949	10.2	1959	9.5	-0.7	-1.35
Berlin	1947	9.4	1958	8.7	-0.7	-1.89
Budapest	1949	11.7	1958	10.9	-0.8	-2.45
Vienna	1949	10.1	1959	9.6	-0.5	-1.00
Charleston	1935	19.0	1959	17.9	-1.1	-3.26
New Haven	1949	11.0	1956	10.4	-0.6	-1.03
Hohenpeissenberg	1949	7.0	1966	6.1	-0.9	-2.82
Kremsmünster	1947	9.0	1959	8.1	-0.9	-2.74
Genova	1946	16.3	1958	15.4	-0.9	-2.50

References

Bach, W. and *Jain, K.*, 1991: From climate crisis to climate protection. Greenpeace Germany, Muenster Univ.

Brazdil, R., Kozuchowsky, K., Marciniak, K. and *Tam, T.N.*, 1987: Variation of annual air temperature in Europe in the period of 1881-1980. Climatic Changes, Brno, 115-130.

Budyko, M.I., 1982: The Earth's Climate: Past and Future. Academic Press, London.

Budyko, M.I., Ronov, A.B. and *Yashin, A.L.*, 1987: *History of the Earth's Atmosphere*. Springer Verlag, Berlin.

Energy and Climate, 1977: National Academy of Sciences, Washington D.C.

Götz, G., 1983: Introduction to general climatology. Lecture notes, Orsz. Meteorológiai Szolgálat, Budapest.

Houghton, J., 1994: *Global Warming. The Complete Briefing*. Lion Publishing, Oxford.

Keil, K., 1961: Zum Thema Klimaschwankun-

Keil, K., 1961: Zum Thema Klimaschwankungen. *Meteorologische Rundschau 14*, Jg. Heft 6, 180-182.

Koppány, Gy., 1989: *Atmospheric Resources* (in Hungarian). JATE, Szeged.

Lockwood, J.G., 1986: *World Climatic Systems*. Edward Arnold Ltd., London.

Pivovarova, Z.I., 1970: Study of the regime of atmospheric transparency. Radiation including satellite techniques. *WMO Technical Note 104*, 181-185.

Réthly, A., 1947: Climate of Budapest (in Hungarian). A Budapesti Központi Gyógy- és Üdülőhelyi Bizottság Rheuma- és Fürdőkutató Intézete Kiadványa, Budapest.

Schönwiese, Ch. D., 1988: Volcanic activity parameters and volcanism-climate relationship within the recent centuries. *Atmosfera 1*, 141-156.

World Weather Records, 1971. Washington, D.C.

IDŐJÁRÁS

Quarterly Journal of the Hungarian Meteorological Service
Vol. 98, No. 4, October–December 1994

Determination of the value of atmospheric drought

G. Szász

Debrecen Agricultural University,
P.O. Box 36, H-4015 Debrecen, Hungary

(Manuscript received 4 August 1994; in final form 7 December 1994)

Abstract—The value of atmospheric drought is determined by the temperature and the relative air humidity. Its value expresses the deviation of a given potential evaporation from the ecologically adequate standard value.

The value of atmospheric drought (D_a) under different climates ranges between 0–200. The diurnal course and the intervals of its values are directly proportional to the enthalpy. The reference values of the equations used for estimation can be chosen optionally. The atmospheric drought value can be considered as a meteorological and ecological index. This paper presents tables and nomograms which demonstrate how to calculate it.

Key-words: atmospheric drought, atmospheric dryness, enthalpy, potential evaporation, Debrecen.

1. Introduction

When speaking about drought, a distinction has to be made between soil drought and atmospheric drought (or atmospheric dryness). Soil drought is an extreme case of the water balance in the soil, while the atmospheric drought is an extreme event of the physical conditions of boundary layer. There are great differences between the duration of soil and atmospheric drought. If considered by its harm causing effects, the duration of soil drought averages $2–10 \times 10^2$ hours, whereas the same average for atmospheric drought is 2–6 hours/day and usually is formed around noon. Atmospheric drought in ecological and agricultural sense is when the relative humidity falls below 40%. It has to be remarked that this critical value is not considered constant either in climatological or in ecological respect. Below, the possible way of the numerical estimation of the atmospheric drought will be discussed.

2. *Theoretical basis*

The specific enthalpy of air under about the same pressure is the sum of the sensible and latent heat:

$$E = c_p \cdot \rho_a \cdot T + [L_a(0.622 \cdot e/p)] \qquad (\mathrm{J\ kg^{-1}\ K^{-1}}), \tag{1}$$

where c_p is specific heat at constant pressure (1 J $\mathrm{kg^{-1}\ K^{-1}}$), ρ_a air density (1.2 kg $\mathrm{m^{-3}}$), e vapour pressure (hPa), L water evaporation heat (20°C = 2.5 MJ $\mathrm{kg^{-1}}$), T is temperature (K). This equation corresponds to the first axiom of thermodynamics (*Götz* and *Rákóczi*, 1981). The degree of atmospheric drought (D_a) can be characterized by the quotient of the latent and sensible heat:

$$D_a = \frac{c_p \cdot \rho_a \cdot T}{L \cdot \rho_a (0.622 \cdot e/p)}. \tag{2}$$

This quotient has a minimum for each T which is formed at a saturation vapour pressure (E) when $e = E(T)$. The value of air humidity at this point:

$$D_{a\ \max} = \frac{\rho_a \cdot c_p \cdot T}{L \cdot \rho_a (0.622\, E(T)/p)}. \tag{2.a}$$

To express the joint value of sensible and latent heat, the equivalent temperature (Θ) is used (*Gates*, 1980):

$$\Theta = T + e/\gamma, \tag{3}$$

where γ is psychrometrical constant:

$$\gamma = \frac{c_p \cdot p}{0.622 \cdot L} = 0.66 \quad (\mathrm{hPa\ °C^{-1}}).$$

So, by the equivalent temperature, the humidity of air can be determined:

$$D_a = t/(e \cdot 0.66). \tag{4}$$

The expression above is a ratio based on thermodynamics and is particularly well suited to determine the degree of the atmospheric drought if the temperature in the numerator is expressed in K. The denominator in Eq. (4) will grow in range as temperature rises, and, so, the function will tend to fall if the e/E ratio is low. This means that with the increase of air drought, the D_a value will proportionally fall. Consequently, the quotient of the two terms determining the

value of equivalent temperature in Eq. (4) expresses a specific thermodynamical state, which, on the one hand, is inversely proportional to relative air humidity and, on the other, effects the numerical value of humidity to a slight extent only. Therefore, it is not fitted for the practical definition of air drought, since it does not express the sensible and latent heat extractions and, so, can only be considered as a stationary characteristic.

The value of atmospheric dryness is a very significant value in physical and also in ecological sense. To determine its value, the formula of potential evaporation (PE_0) can be used as a starting point, which is (*Szász*, 1973):

$$PE_0 = a[f(v) \cdot 0.0054\,(t + 21)^2\,(1 - e/E)^{2/3}] \quad \text{mm}, \tag{5}$$

where t is daily mean temperature (°C), e/E saturation ratio, v daily average wind speed (m s^{-1}), $f(v)$ effect of wind speed, a the factor correcting the microadvectional effect. The latter is needed because the constant of the formula was determined by pan evaporation measurements (a = 0.85–1.00). This equation is valid for 2 m s^{-1}. So, the calculation is made by the evaporation according to the temperature and the water vapour saturation ratio. A parabola function can be used to describe the potential evaporation determined by the temperature:

$$PE_0\,(t) = a\,(t - t_0)^2. \tag{6}$$

In this function the apex of the parabola is on axis x. This criterion expresses that the minimum of PE_0 (t) equals 0. If the square roots of both sides of the equation are extracted:

$$\sqrt{PE_0} = \sqrt{a} \cdot t - \sqrt{a} \cdot t_0, \tag{7}$$

i.e. $\sqrt{PE_0}$ is a linear function of t temperature. The line characteristics fitting the experimental measurements perfectly are $r^2 = 0.9990$, $a = 0.005356$, $t_0 = 20.89 \approx 21$ °C. For relative humidity the following relationship was found to be adequate:

$$\log PE_0\,(e/E) = \log a' + b \log (1\text{–}e/E),$$

i.e. the logarithm of PE_0 is the linear function of the logarithm of the (1–e/E) value. The test of the calculation results shows that

- the correlation can be considered linear,
- by the fittings based on experimental measurements the lines are parallel, i.e. the direction tangent of the lines in the examined interval is independent of the temperature (5–40 °C).

Based on the statements above, $b = 0.06645$, the determination coefficient $r^2 = 0.005$.

These calculations led us to the interpretation of the role of temperature and saturation ratio in the degree of evaporation.

3. The definition of atmospheric dryness

There exists no physically defined value for atmospheric drought used in practical sense in agrometeorology and in other related fields of science, though there has been a high demand for it (*Munn*, 1970; *van Eimern* and *Häckel*, 1979). The frequency of parallelism between temperature (= 30°) and relative humidity (= 40%) was examined by *Rákócziné Wagner* (1976) in 12 data series between 1930–1960. She concluded that, in Hungary, the frequency is the highest in July and August in 10–25% intervals. *Slatyer* (1963) and *Cary et al.* (1968) investigated the water movement in plants under dry conditions. They found that the physical state and mobility of the water in the plant, in the vascular tissues in particular, are closely correlated with atmospheric dryness. The hydrical state, the growth and, consequently, the productivity of a plant are determined by the frequency value of the water potential in the air and plant foliage *(Kreeb*, 1963; *Bierhuzien* and *Slatyer*, 1965; *O'Leary* and *Knecht*, 1971). Results of national and international research support the view that the numerical expression of the atmospheric dryness is an actual demand by meteorologists and ecologists. To define the numerical value of the atmospheric dryness, we used the product of the following proportions as a starting point

$$D_a = 100 \frac{t_a}{t_{25}} \cdot \frac{(e/E)_a}{(e/E)_{40}} = \frac{PE_a}{PE_{0\,ref}}, \tag{9}$$

where D_a is a value without dimension to express the degree of atmospheric dryness, t_a and $(e/E)_a$ are air temperature and saturation ratio, t_{25} and $(e/E)_{40}$ the temperature and saturation ratio at a given time, PE_a potential evaporation with different temperature and saturation ratio values, PE_{0ref} potential evaporation with temperature: 25 °C and saturation ratio: 0.4. As atmospheric dryness tends to be formed around noon, the reference values were selected accordingly. The reference values can be optional, depending, though, on the type of the ecological system (e.g. hydromorph, xeromorph). As the drying effect of the various elements is different, instead of their direct values, the proportions of the values of Eq. (5) are being compared,

$$t_{25} = 0.0054\ (25 + 21)^2 = 11.43$$

$$(e/E)_{40} = (1 - 0.4)^{0.67} = 0.71.$$

In the estimations these two reference values were used. The product of the temperature and of the evaporation value (determined by the saturation ratio) expresses the evaporation conditions of these two values and the size of resultant evaporation. Eq. (5) proves that the effect of the two elements in the process of evaporation is different, which is expressed by the difference in the exponents and by the order of magnitude of the coefficient of the two elements *(Fig. 1)*. The above impact functions are fitted for the numerical expression of atmospheric dryness:

$$D_a = 100 \frac{(0.0054 \cdot t + 21)^2}{11.43} \frac{(1 - e/E)^{0.67}}{0.71} .$$

The denominator involves the function of the temperature (25°C) and the saturation ratio (0.4), which supply the basis of the correlation.

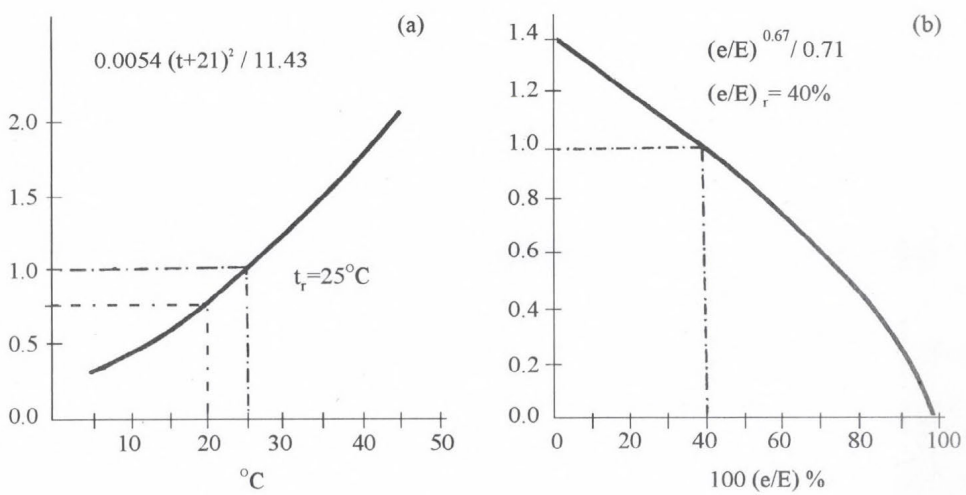

Fig. 1. Calibration curve for effectivity of the temperature (*a*), effectivity of the saturation ratio (*b*).

According to the estimations, relative atmospheric dryness is increased by a decrease in temperature and by an increase in relative humidity. *Table 1* shows the impact function of temperature and saturation ratio (in percentage), well representing the contraversary changes that go with the increases of the two elements. It can be concluded that the atmospheric dryness value (D_a) expresses an evaporation ratio compared to any optional reference value, as the numerator represents atmospheric evaporation potential, whereas the denominator is a standard value (25°C, 40%). The quotient expresses the deviation from the standard value.

Table 1. Atmospheric dryness values in Debrecen

°C	e/E (percentage)									
	10	20	30	40	50	60	70	80	90	100
5	0.42	0.38	0.36	0.32	0.28	0.24	0.20	0.15	0.10	0
10	0.59	0.54	0.50	0.45	0.40	0.34	0.28	0.22	0.14	0
15	0.80	0.74	0.68	0.61	0.54	0.46	0.38	0.29	0.18	0
20	1.03	0.96	0.88	0.79	0.70	0.60	0.50	0.38	0.24	0
25	1.31	1.21	1.11	1.00	0.89	0.76	0.63	0.48	0.30	0
30	1.61	1.49	1.37	1.23	1.09	0.93	0.77	0.59	0.34	0
35	1.94	1.81	1.64	1.48	1.32	1.12	0.93	0.71	0.44	0
40	2.29	2.12	1.94	1.75	1.56	1.33	1.10	0.84	0.53	0
45	2.70	2.49	2.29	2.06	1.83	1.57	1.30	0.99	0.62	0

The atmospheric dryness value is a complex climatic parameter whose graphical representation facilitates estimation making (*Fig. 2*).

As the formula exists for temperatures down to –11 °C, the dryness value can be used in a diversity of regions.

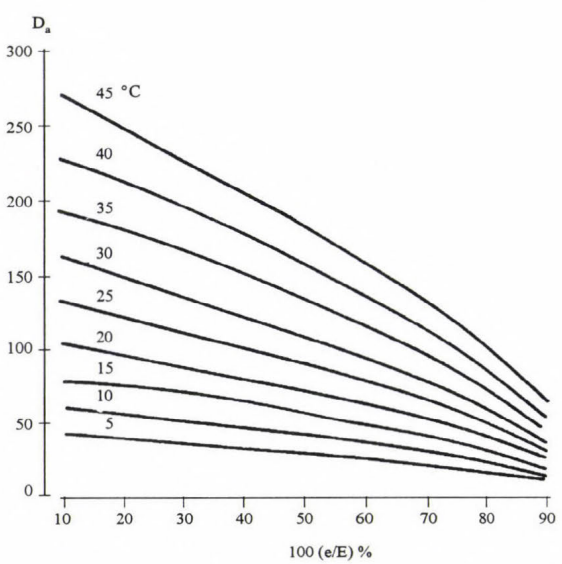

Fig. 2. Nomogram for the determination of the atmospheric dryness (D_a) from the temperature and relative humidity values.

4. Discussion

The atmospheric dryness value introduced above is well fitted for climatic and agro-meteorological investigations. Dryness is usually described by the

deficiency of rainfall. It has to be stressed, however, that the deficiency of rainfall could be seriously worsened by atmospheric dryness which is manifested by high temperature and low relative humidity. Atmospheric dryness is usually very heavy at midday, which produces adverse climatic and ecological conditions for plants with high water requirement. There are significant regional differences in this respect, especially in dry and hot periods. The values of air humidity and atmospheric dryness are considerably different in various climatic zones. Let us consider some examples proving the feasibility of the value in question.

Atmospheric dryness value strongly depends on the climatic zones and is closely related to rainfall. *Fig. 3* shows the precipitation and temperature data of representative areas of 8 different climatic zones (*Péczely*, 1984). The part of the figure dealing with temperature represents annual average fluctuation. The fluctuations of the atmospheric dryness values, determined by the monthly temperature average of the coldest and warmest months can be seen at the bottom figure (*c*). The covering curve involving the lower and upper values gives a synoptical representation of the annual fluctuations in the different climatic zones. Giving a detailed global analysis of the examined value does not belong to the subject of this paper, this figure, however, convincingly proves

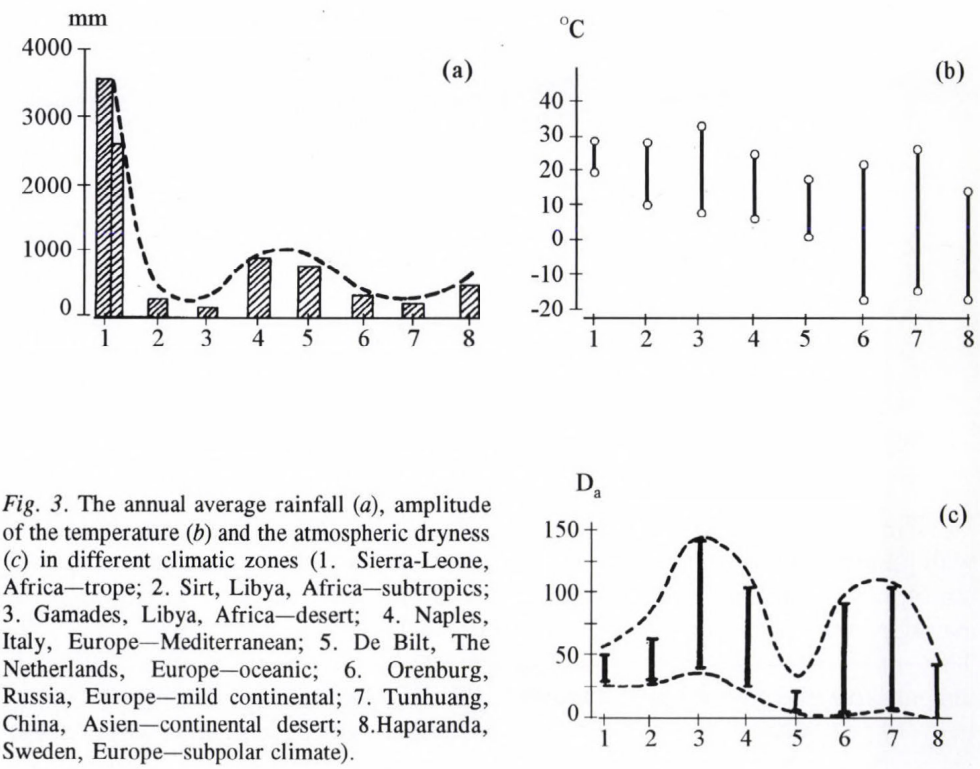

Fig. 3. The annual average rainfall (*a*), amplitude of the temperature (*b*) and the atmospheric dryness (*c*) in different climatic zones (1. Sierra-Leone, Africa—trope; 2. Sirt, Libya, Africa—subtropics; 3. Gamades, Libya, Africa—desert; 4. Naples, Italy, Europe—Mediterranean; 5. De Bilt, The Netherlands, Europe—oceanic; 6. Orenburg, Russia, Europe—mild continental; 7. Tunhuang, China, Asien—continental desert; 8.Haparanda, Sweden, Europe—subpolar climate).

its feasibility. The regional distribution of atmospheric drought values can help to draw the boundaries of the different plant-ecological regions. Each fraction of the family of curves in Fig. 2, in fact, represents different climatic characteristics. *Fig. 4* is an attempt to locate the different climatic and ecological regions according to their atmospheric dryness values and the fluctuation of temperature.

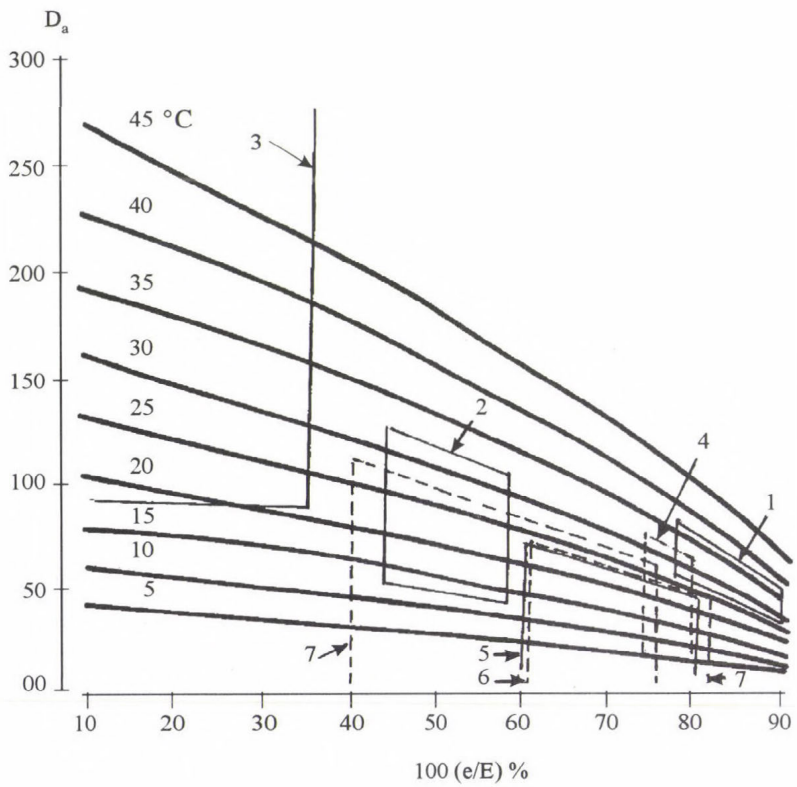

Fig. 4. Surfaces and dividing boundaries of different climatic zones in the D_a nomogram.

The atmospheric dryness values provides scopes for analyses in a given area with heterogenous climate. *Fig. 5* shows the regional distribution of the atmospheric dryness value calculated from the daily maximum temperature averages and the average relative humidity at 14 UTC in July from 1901–50. This map gives a good representation of the consequent effect of high temperature and low relative humidity. The highest atmospheric dryness value in every two maps is formed in the southernmost parts of Hungary, whereas the

lowest relative humidity values come from the middle but not the hottest parts of the country. A similar conclusion can be drawn from Fig. 5a. In this case the value of temperature was calculated from the average absolute maximum and the 14 UTC relative humidity values reduced by 5%. Compared with Fig. 5b, it can be concluded that in the Fig. 5a the dryness values are 50–60 units higher, but there is no significant difference between their geographical distribution. It is commonly known, that in the Carpathian-basin the highest atmospheric drought values are formed in July, that is why our attention was basically focused on the detailed analysis of this period.

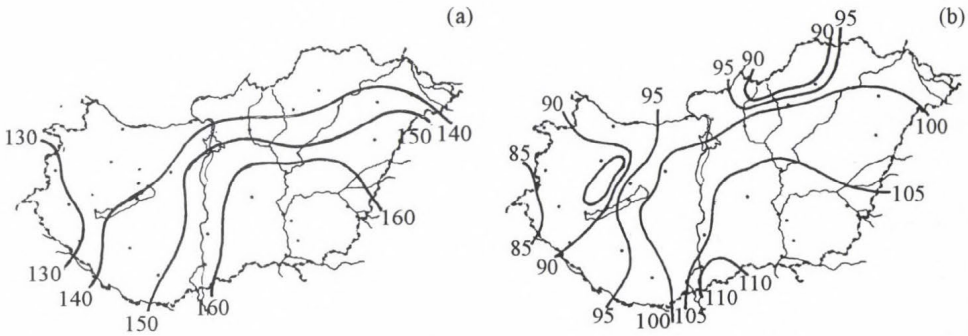

Fig. 5a. Values of the atmospheric dryness from the average absolute temperature maximum and minimum relative humidity (14 UTC) in Hungary (1901–1950).

Fig. 5b. Values of the atmospheric dryness from the average temperature maximum and relative humidity (14 UTC) in Hungary (1901–1950).

The atmospheric drought values for Debrecen are fairly near the average values common in the Hungarian Great Plain. This is why the data observed in Debrecen are demonstrated here:

July:

daily temperature average:	20.7°C
daily fluctuation average:	±6.1°C
average relative humidity:	68%
daily fluctuation average:	±15%
daily average maximum dryness value:	92.5
daily average minimum dryness value:	44.1
average atmospheric dryness:	68.3

A comparison made between the latter value and the D_a interval in column six, Fig. 4, suggests that the continental character of the Hungarian plain in summer is regulated by influences of continental climate.

Atmospheric dryness values vary within a wide range. To increase information in this respect, the frequency of daily dryness averages for the years 1951–1990 was established (*Table 2*). The estimated values are placed in vary wide intervals, which indicates that there is an alteration of continental and ocean predominance.

Table 2. Frequency of atmospheric dryness value calculated by daily averages

D_a	Number of day	Frequency, %
> 10	1	0.08
11 - 20	28	2.26
21 - 30	74	5.97
31 - 40	167	13.47
41 - 50	239	19.27
51 - 60	254	20.48
61 - 70	239	19.27
71 - 80	143	11.53
81 - 90	49	3.95
91 - 100	35	2.82
101 - 110	8	0.65
111 - 120	2	0.16
121 - 130	1	0.08
Sum	1240	100.00

The extremes of drought values in Hungary (*Climatic Atlas of Hungary*, 1967) run between 0–193. The dryness values reflect the climatic conditions, so, high extremes may follow each other. The very heavy drought spell of the summer of 1983 was characterized by sharp fluctuations in temperature and moderate changes in the relative air humidity. The quick change in the atmospheric drought values can be attributed to the effect of advection regulated by synoptic weather processes. *Fig. 6* is an example of this, showing the atmospheric dryness values estimated by values measured at 14 UTC on 17 days of a very hot summer (1983). On the first 7 days there was dominated subtropical continental air mass (NE-Africa), its predominance was broken by an attack of cold air front from the North-Atlantics.

The diurnal change in the atmospheric dryness values is the result of temperature cycles, as shown in *Fig. 7*. The solid curve demonstrates the average diurnal course in July, with the parameters belonging to the extreme values also are represented. The dashed curve indicates the diurnal course of the atmospheric dryness in a hot, dry period. The difference between the two diurnal courses supports the extreme character of the climatic conditions in Debrecen.

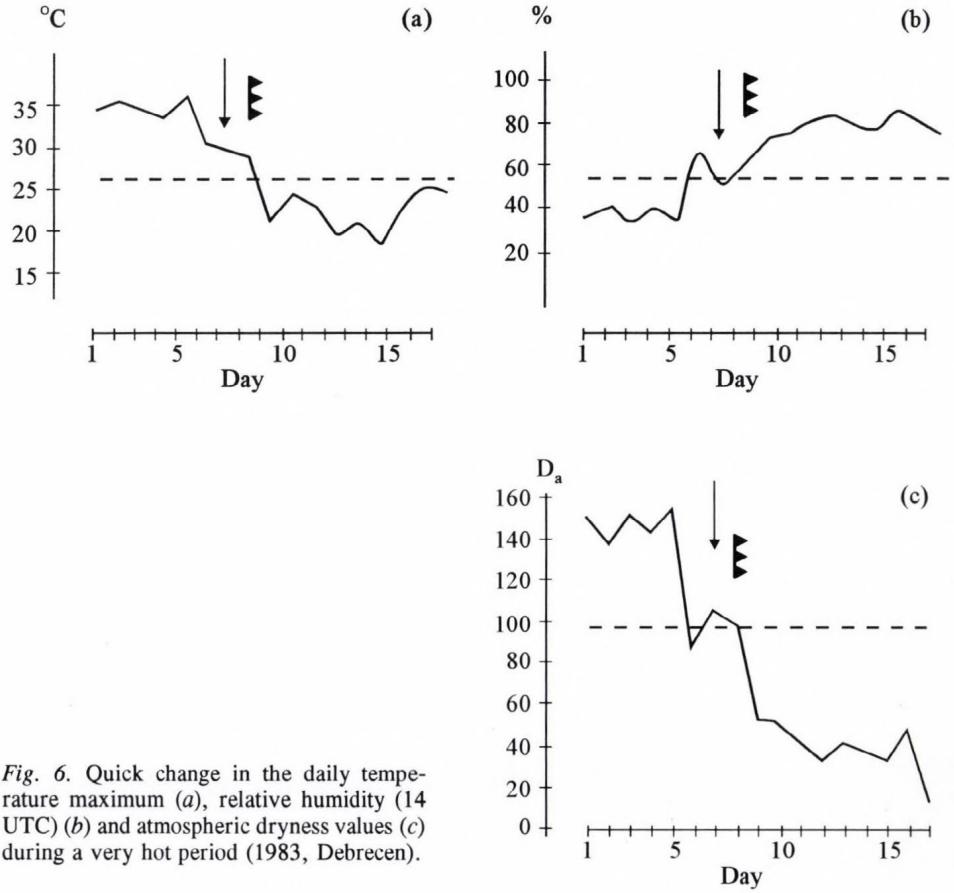

Fig. 6. Quick change in the daily temperature maximum (*a*), relative humidity (14 UTC) (*b*) and atmospheric dryness values (*c*) during a very hot period (1983, Debrecen).

5. Conclusions

The atmospheric dryness value is a proportion which can physically be deduced: in fact, it is the ratio between the value calculated by the $t = 25°$ and $e/E = 0.4$ and the existing potential evaporation. We assume that relative air humidity exclusively does not provide sufficient basis to determine the atmospheric dryness value. The definition should be based on the theory that increasing temperature results an increase in the water vapour saturation interval. That is, the degree of dryness is effected by the temperature as well, the saturation water vapour pressure, which is increasing as the temperature is rising. Air water potential is dependent on the air temperature and the vapour saturation ratio. The temperature component of the water potential: $(\rho W/M \cdot RT)$, where W is water molecule weight, R gas constant (8.3143 J K^{-1} mol^{-1}). This value is only slightly affected by the temperature. The water potential value changes according to the logarithm of the saturation ratio mainly, and so,

of two factors determining evaporation, vapour saturation ratio should be taken priority. To bridge this difference in their importance we used Eq. (5), which contains the product of temperature and air humidity evaporation potential. This multiplicative linkage makes the widening of the scales also possible. So, the product of the effect ratio of the two meteorological elements is fit to truely express atmospheric drought conditions.

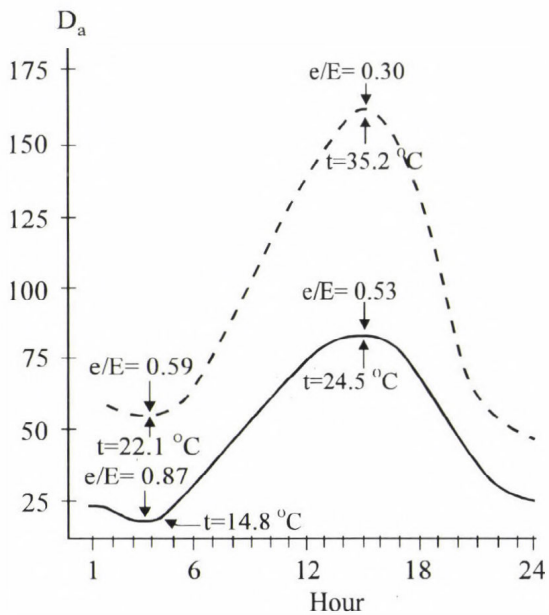

Fig. 7. Diurnal course of the average (solid) and maximum (dashed) atmospheric dryness in Debrecen.

Atmospheric dryness is a relative value in ecological sense as well. The atmospheric dryness value, naturally, allows high temperature and low relative humidity for drought-resistant plants, the inverse of which is true for plants with high water requirement. Taking temperate zone conditions, 25°C and a relative humidity of 40% can be considered as reference values for mezophyte requirements, so they are fit for general use. The advantage of estimation is that the product of atmospheric dryness ratio is applicable for different ecological conditions, however, the value intervals calculated by the previously discussed method also fit into the hydric cathegories:

— hydrophytic $D_a = 0 - 75$,
— mezophytic $D_a = 25 - 100$,
— xerophytic $D_a = 50 - 200$.

The above intervals vary in a wide interval for the reason that temperature has also been involved.

The above mentioned results are well applicable for agrometeorological, agroclimatological and ecological researches.

References

Bierhuzien, J.F. and *Slatyer, R.O.*, 1965: Effect of atmospheric concentration of water wapor and CO_2 in determining transpiration – photosynthesis relationships of cotton leaves. *Agric. Meteorol. 2*, 259-270.

Cary, J.W., Jensen, M.E. and *Fisher, H.D.*, 1968: Physical state of water in plant xylem vessels. *Agron. Journ. 60*, 167-169.

Climatic Atlas of Hungary, vol. II, 1967. Akadémiai Kiadó, Budapest.

Eimern, van J., Häckel, H., 1979: *Wetter- und Klimakunde*. Ulmer Verlag, Stuttgart.

Gates, M.D., 1980: *Biophysical Ecology*. Springer Verlag, New-York-Heidelberg-Berlin.

Götz, G., Rákóczi, F., 1981: *A dinamikus meteorológia alapjai*. Tankönyvkiadó, Budapest. 483 p.

Kreeb, K., 1963: Hydrature and plant production. In The Water Relations of plants (eds.: *A.J. Rutter* and *F.H. Wintehead*). Blackwell Sci. Publ., London.

Munn, R.E., 1970: *Biometeorological Methods. Environmental Methods*. Academic Press, New-York and London.

O'Leary, J.W. and *Knecht, G.N.*, 1971: The effect of relative humidity on growth, yield and water consumption of bean plants. *J. Amer. Soc. Hortic. Sci. 96*, 263-265.

Péczely, Gy., 1984: *Climate of the Earths* (in Hungarian). Tankönyv Kiadó, Budapest.

Rákócziné Wágner, M., 1967: *Complex-Climatological Investigation of Atmospheric Drought* (in Hungarian). *Időjárás 71*, 34-39.

Stocker, O., 1960: Physiological and morphological changes in plants due to water deficiency. In *Arid Zone Research*. UNESCO XV., Paris, 63-104.

Szász, G., 1973: A new method of estimating potential evapotranspiration (in Hungarian). *Hidrológiai Közlöny*, 435-442.

IDŐJÁRÁS

Quarterly Journal of the Hungarian Meteorological Service
Vol. 98, No. 4, October–December 1994

Brief survey on recurrences of extreme rainfalls in Genoa, Italy

G. Russo and **A. Sacchini**

Department of Earth Science, University of Genoa,
V. le Benedetto XV 5, Genoa, Italy

(Manuscript received 17 February 1994; in final form 16 November 1994)

Abstract—This paper is a brief survey on extreme rainfalls (considered as precipitations of remarkable intensity with overflowing phenomena) recorded at the University Meteorological Observatory of Genoa in the last 100 years. We found that meteorological phenomena similar for causes (intense precipitation) and effects (floods) don't follow any particular cycle as regards their return periods and they are not linked to climatic periods particular for their rainfall or droughtiness. The years of the events, associated with different intensity of precipitation in the Standardized Distribution are distributed into 4 'pairs'. Temporal steps between events of the same 'pair' or extreme rainfalls cycle (λ = 8, 15, 22, 25 years) increase with the growing up of the annual precipitation; these intervals can be associated with a precise exponential sequence. Finally, according to this survey method, return periods of new possible extreme events are proposed.

Key-words: standardized distribution of annual precipitations, flood events, Genoa.

1. Introduction

On September 27th, 1992 a torrential precipitation caused the overflow of many streams flowing through Genoa; there were deads and damages. Meteorological characteristics of last flood have been rather similar to other tragic events occurred in the last 40 years; the meteorological causes of these exceptional rainfalls were studied by many authors (*Bossolasco et al.*, 1970, 1971; *Dagnino et al.*, 1975, 1978). Flood events from 1957 to 1992 developed according to the same dymanics represented in *Fig. 1*:

— an Atlantic disturbance over Spain, bringing cold air as joined to a deep depression in the north-western sectors of Europe;
— stopping action towards the eastern sectors by an anticyclonic ridge located over Balcans;

— this blocked disturbance conveys warmer and wetter southern air, flowing towards this frontal system against Ligurian Appenninic range so that very intense and concentrated orographic and frontal precipitations fall over on north-western Italy.

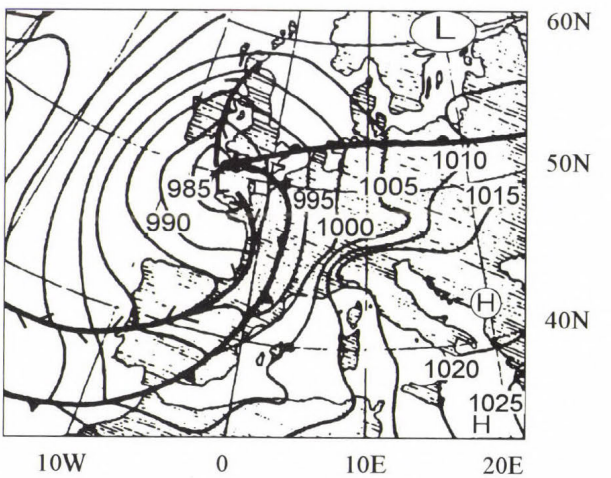

Fig. 1. Weather map during 1977 event and typical of extreme rainfalls events in Genoa (after Europäischer Wetterbericht of Deutscher Wetterdienst).

In this work we don't consider the already studied mechanisms generating these phenomena, but we investigate their recurrences and the possibility to forecast the existence of particular climatological epochs favouring these events. Considering return frequences of extreme rainfalls, we can say these events are not so rare in Genoa and a planetary control system, not even surely known, exists. The possibility of forecasting long term returns of these events is very complex; floods are the consequence of more circumstances like 'a prolonged period, or close succession of periods, of large-scale precipitation; severe transitory storm; violent convective activity' (*WMO, GARP,* 1975).

2. Data and methods of analysis

In *Table 1* all the years and months are shown in which heavy precipitations occurred; we consider those events memorable for their unusual intensity (mm/h) and for damages brought about to the community, such as stream overflowings, landslides and victims.

Table 1. Extreme rainfalls in Genoa, precipitation amount and intervals in years between the successive events from 1892

Year	Date	Day	Event	Total precipitation (mm)		Breaks
				Month (1)	Year (2)	
1892	October	6	181.3	358.3	1445.2	0
1907	October	24–25	246.1	599.4	1362.9	15
1926	October	21–22	86.7	215.7	2008.8	19
1945	October	29–30	275.8	352.0	1127.8	19
1951	November	7–8	396.4	597.6	1990.8	6
1953	September	19	218.6	489.0	1210.0	2
1970	October	7–8	449.2	454.4	1641.6	17
1977	October	6–7–8	370.0	490.6	2189.8	7
1992	September	27–28	450.8	551.0	1690.0	15

(1) Monthly averages: September 113.6 mm, October 202.4 mm, November 170.6 mm
(2) Annual mean: 1287.9 mm

It may be observed that the probability of rainy days with extreme precipitation amounts in Genoa is very high in the beginning of autumn; in particular, October presents the higher occurrence for extreme rainfall events. At the end of dry season (from the end of September to the beginning of November), the Azore's high pressure, bringing a long period of good weather in summer, in the Mediterranean area, is subject to a rapid collapse (equinoctial perturbations) with infiltrations of polar maritime air under complex interactions of different oceanic and continental effects and violent circulation between land and sea (*Bossolasco et al.*, 1973). In October, in particular, the unstable air masses (northern polar maritime air and southern warm, wet maritime air) happens to bear intense frontal and orographic precipitations in the Ligurian Appennine.

As a matter of fact in October six of nine flood events were recorded in the last 100 years; the others occurred about the end of September or the first days of November. Even ancient Genoese chronicles report big flood events in 1402 and 1822, both of them in October (*Giustiniani*, 1407; *Gazzetta di Genova*, 1822).

In Table 1 there are also included total precipitations, occurred in the month and in the year of the event; this helps to understand the importance of the events compared to monthly and annual precipitation amounts. It is worth

underlying on October 7–8, 1970 there was a rainfall of 449.2 mm equivalent to the 98.9% of the precipitation fallen in all the month. In the last column interval periods among floods are shown; evident recurrences are not present. Other authors applied numerical analysis to the precipitation series of Genoa looking for periodic recurrences (*Flocchini et al.*, 1981; *Flocchini*, 1983) by using the DFT (Discrete Fourier Transform); they found maximum spectral densities around 22 years, generally ascribed to sunspots cycles and planetary phenomena.

We wanted to verify the hypotesis that each event is associated with a climatic discriminant linked to the historical trend of precipitation series, i.e. the event occurs in a very rainy year or that happens in a rather normal or drought year. So we analysed the trend of annual departure of precipitations from the mean for the historical series of Genoa (*Fig. 2*). Arrows point out the years of the events with their annual departure from the mean (1287.9 mm). Comparisons between Fig. 1 and Table 1 allow to say that there are not climatic periods in which flood events exclusively occur. The curve of Standardized Cumulative Distribution of total annual precipitation amounts has been built (*Fig. 3*). This is the procedure we follow to point out whether a correlation between floods and particularly distinguishable climatic periods (rainfall or droughtiness) exists.

In the curve we group single events according to precipitation amount of the year of occurrence (see Table 1) to verify single event position in comparison with the mean value, considering their variability or standard deviation from the mean. The curve shows a slight asymmetry towards maximum values of precipitation; in 1872 the absolute maximum value of the whole historical series (2872 mm) was recorded, although without flood events.

Fig. 3 points out that the events occur irregularly in the curve but they seem to group in 'pairs' or 'trios', distant from the mean with a different standard deviation; the arrows show distances λ (years) among events of the same cluster (λ = 8, 15, 22, 25-26 years). The clusters ('pairs') are distributed in the curve prevalently joined to annual precipitation amounts superior to the mean; in fact, the main recorded events (1970, 1977, 1992) took place during many rainy periods; the 'pair' 1945-1953 has an exception, because it's associated with annual precipitations a little inferior to the mean.

The following *list* has been worked out to classify different climatic periods, which analysed flood clusters are associated with:

1. * 1945-1953, two events:
- pair W.D. (Weakly Dry):
- recurrences in the cluster every 8 years;
- precipitation amount of the year of occurrence a little inferior to the mean; standard deviation 0.5;
- this series ended in 1953.

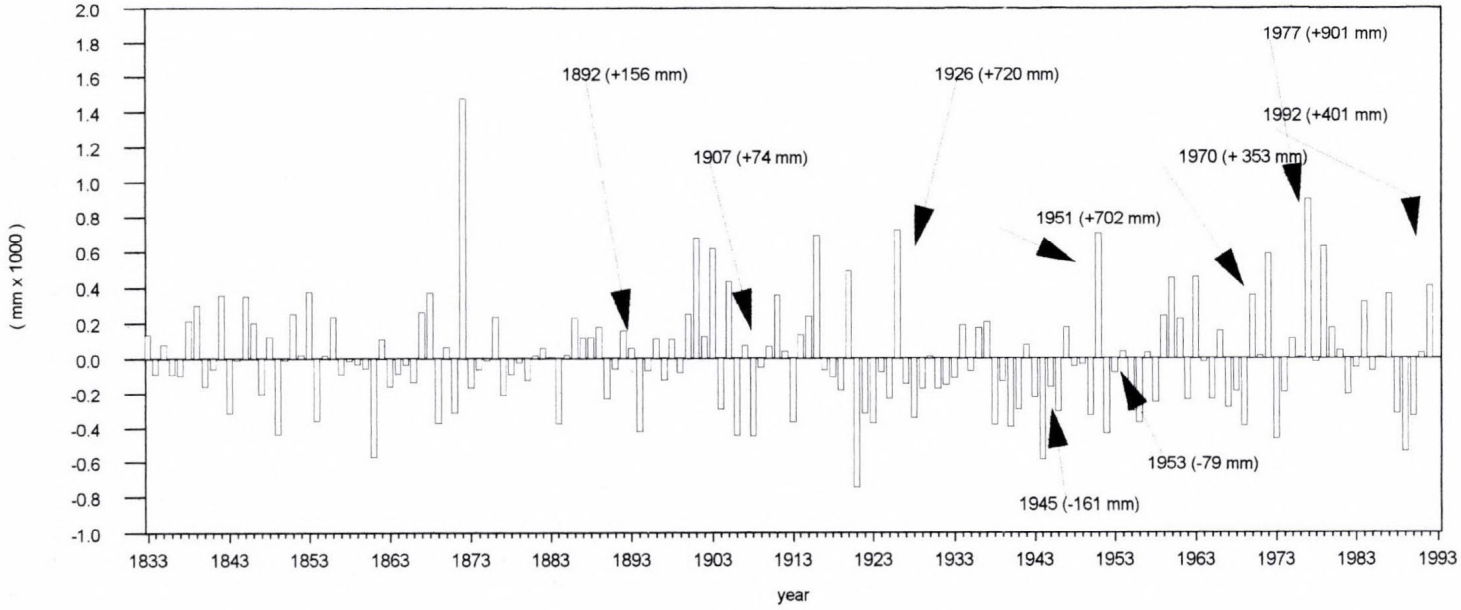

Fig. 2. Departure from the mean of annual precipitation amounts in Genoa (1833–1992); arrows point out last hundred year flood events.

2. * 1892-1907, two events:
- pair W.R. (Weakly Rainy):
- recurrences in the cluster every 15 years;
- annual precipitation amounts a little superior to the mean; standard deviation 0.5;
- this series ended in 1907.

3. * 1970-1992, two events:
- pair I.R. (Intensively Rainy):
- recurrences in the cluster every 22 years;
- annual precipitataion amounts superior to the mean; standard deviation 1.5;
- events which could probably appear 22 years after 1992 event, in 2014.

4. * 1926-1951-1977, three events:
- pair V.I.R. (Very Intensively Rainy):
- recurrences in the cluster every 25 years;
- annual precipitation amounts much superior to the mean; standard deviation 2.5;
- there is the possibility that periodicity has not still ended: probably the next flood event of this kind may verify in 2003-2004.

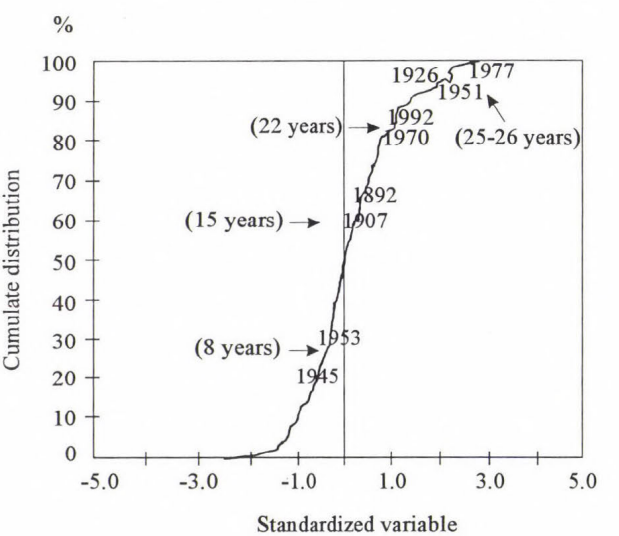

Fig. 3. Representation on the Standardized Cumulative Distribution of total annual precipitation and positions of extreme rainfalls; in parentheses intervals between the successive events similar for distance from the mean of their total annual precipitation are given.

Results show that extreme events, even if equivalent in their metorological background, are different for three factors:

(1) these events are clusterizable according to climatic periods different for annual precipitation amount;
(2) the events distribute in 'pairs' pointing out the beginning and the end of a single flood cycle: all pairs are ended except for 1977 ($\lambda = 25$ years: this pair will be likely to end in 2003);
(3) recurrences periods of every cycle increase with the growing up of the precipitation amount of the year of occurrence.

Sequence T between intervals of similar events seems to follow an exponential progression like $n^{\sqrt{2}}$ where $n = 1, 2, 3...$(*Table 2* and *Fig. 4*); in Table 2 comparisons among theoretical and experimental intervals are reported together with a classification of the events. It's intersting to note that, in the series we can analyse that extreme rainfall events don't fill in the 'n' positions available in the table; we suppose that, if the criterion we adopted (that every event may belong to different climatic patterns measurable through annual trend of precipitation amount) is associated with a physical reality of temporal successions, other 'n' extreme rainfalls cycles, we could not verify, may virtually exist.

Table 2. Clusters of extreme rainfall events according to rainfall or droughtiness of the year of occurrence, intervals in years between elements of the same group and their positions on the extrapolation curve

n	Intervals		Clusters		Years
	Computed	Real			
1	1.0	?	V.I.D.	(very intensive dry)	
2	2.7	?	I.D.	(intensive dry)	
3	4.7	?	V.D.	(very dry)	
4	7.1	8	W.D.	(weakly dry)	1945, 1953
5	9.7	?	U.D.	(usually dry)	
6	12.6	?	U.R.	(usually rainy)	
7	15.7	15	W.R.	(weakly rainy)	1892, 1907
8	18.9	?	V.R.	(very rainy)	
9	22.4	22	I.R.	(intensive rainy)	1970, 1992
10	26.0	26	V.I.R.	(very intensive rainy)	1926, 1951, 1977
11	29.7	?	U.R.	(unusually rainy)	

Return periods and cycles, presenting periodicities similar to those ones we found, were already ascertained at least for as concerning some river floods in the northern Italy and generally some earth phenomena, such as variations in geomagnetic field declination, annual precipitations, river flows, atmosphere composition (*Rima*, 1962). In particular, we can remember *Mosetti* (1956), who summarized periodicities he found in earth phenomena, establishing a relation between the mean of the observed periods and a theoretical succession according to a geometrical progression of kind $\sqrt{2}$. Besides, it is important to

stress the presence of the 22 year cycle already mentioned, which seems to demonstrate the possible relationship between sunspot cycles and the weather and climate. However, as return periods of found events are also rather different from this particular cycle, we cannot draw precise conclusions in this sense according to the indications of other authors (*Pittock*, 1978a, b).

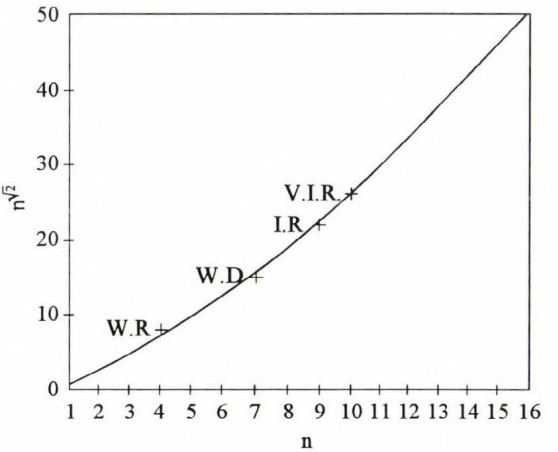

Fig. 4. Positions of clusters of extreme rainfalls events on the extrapolation curve.

3. Conclusive remarks

Even if the number of events is little, results presented lead us to point out some main elements:

(a) flood precipitations occur independently from the climatic period: they are present both in very intensively rainy and in drought periods;
(b) the criterion which associates every annual precipitation amount with the year of occurrence of the extreme rainfall, allows to distinguish 4 different flood clusters;
(c) these clusters appear in 'pairs' marking the beginning and the end of each flood cycle;
(d) distances in years between events of each 'pair' are proportional to the growing up of the Standardized Cumulative Distribution curve of the annual precipitation amount;
(e) distances in years among each flood cluster seem to follow a characteristic numerical succession.

Characteristics of this model don't allow absolute forecastings; anyhow, the method we used can be a contribution to the future research in the field of flood phenomena forecasting.

APPENDIX

On September 23, 1993 another torrential precipitation with overflowing phenomena ensued in Genoa (456.0 mm the precipitation in the event, 519.2 mm monthly amount). The meteorological conditions causing the event were the same of last ones. Trying to include this event in our model, we inserted the annual precipitation amount (1159.6 mm) in the Standardized Distribution. This value inserts the event between 1945 and 1953 in a year W.D. belonging to the 'pairs' with $\lambda = 8$ years. In *Fig. 5* clusters are represented in horizontal layers according to precipitation amount of the occurrence year of events and to their intensity.

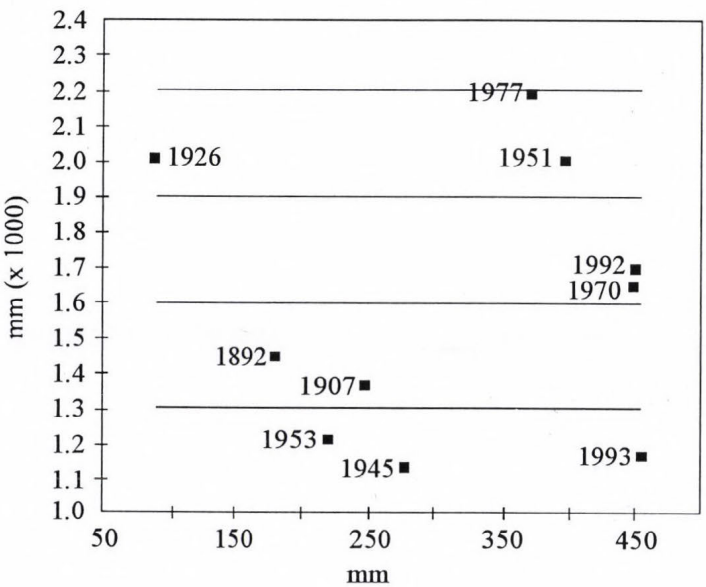

Fig. 5. Representation of years of extreme rainfall events according to their total annual precipitation (abscissa) and intensity of the event (ordinate).

We can suppose that events of the cluster W.D. have started again and so next event will likely ensure in 2001; that, together with the event of cluster V.I.R., expected for 2003, will be likely to lead to appearence of two different 'pairs' in very close years.

Characteristics of this model don't allow absolute forecastings; anyhow, the method we used can contribute to future research in the field of flood phenomena forecasting.

References

Bossolasco, M., Dagnino, I., Flocchini, G., 1970: Situazioni meteorologiche tipiche di precipitazioni forti ed estese sull'Italia Settentrionale. *Geof. e Meteor. XIX, 5-6*, 143-151.

Bossolasco, M., Cicconi, G., Dagnino, I., Flocchini, G.,1971: Le cause meteorologiche della alluvione su Genova del 7-8 ottobre 1970. *Geof. e Meteor. XX, 3-4*, 122-132.

Bossolasco, M., Dagnino, I. and *Flocchini, G.*, 1973: On sea and land climate differences. *Bonner Meteor. Abhandlungen 17*, 467-473.

Dagnino, I., Flocchini, G., Palau, C., 1975: Sulle cause meteorologiche che determinano precipitazioni anomale sulla Liguria. *Atti Acc. Ligure Scienze e Lettere XXXI*, 149-168.

Dagnino, I., Flocchini, G., Palau, C., 1978: Le precipitazioni del 6-10 ottobre 1977 sulla Liguria centrale. *I.T.A.M. 1978*, 267-270.

Flocchini, G., Palau, C., Repetto, I. and *Rogantin, M. P.*, 1981: A mathematical model of the field of precipitation. *Il Nuovo Cimento 1*, 673-681.

Flocchini, G., 1983: On the regularization of the pluviometric series. *2nd Int. Meet. Stat. Climat., Lisbon, September 1983.*

Gazzetta di Genova, 1822: Alluvione. 26 ottobre 1822.

Giustiniani, A., 1407: Annali della Repubblica di Genova; libro IV. vol. II.

Mosetti, F., 1956: Considerazioni preliminari per una legge sulle periodicità naturali. *Tecn. It., Rivista di Ingegneria e Scienze, 8.*

Pittock, A.B., 1978a: A critical look at long term sun-weather relationships. *Rev. of Geoph. and Space Physics 16*, 400-415.

Pittock, A.B., 1978b: Solar cycles and the weather: successful experiments in autosuggestion? In *Solar and Terrestrial Influences on Weather and Climate*. D. Reidel, Dordrecht, pp. 181-191.

Rima, A., 1962: Considerazioni sul periodo undecennale dei fenomeni terrestri. *Geof. e Meteor. X, N. 1, 2*, 34-44.

WMO, GARP, 1975: The physical basis of climate and climate modelling. No. 16, 33.

NEWS

ANNOUNCEMENT

International Conference on Environment and Informatics (EN-IN) in Budapest, Hungary, June 29 – July 1, 1995

International Conference on Environment and Informatics will be organized in Budapest between June 19th and lst July 1995 by the Computer and Automation Research Institute, the Hungarian Academy of Sciences and SCOPE Meeting Co. Ltd. The sponsor of the Conference is the Hungarian Academy of Sciences (HAS) and co-sponsors are Institute for Economic and Environmental Development in Central and Eastern Europe, International Biometric Society, International Council of Scientific Unions (ICSU), International Federation of Automatic Control (IFAC), International Federation of Operations Research (IFORS), International Institute of Applied Systems Analysis (IIASA). The Conference Chairman is academician *I. Láng* (HAS).

The scope of the conference may be formulated as follows:
The management, protection and changes of environment are the most timely, exciting, dynamically developing problems of the day all over the world. In the past years, several global and regional programs have been started in the field of climatic changes, global and environmental changes, acid rains, biosphere, etc. Informatics, information systems, decision support models and mathematical methodology play fundamental role in these research projects.

One of the most significant impediments of the research work is the lack of information on the state and changes of environment. Although projects for the integration of information systems have also been launched, e.g. CORINE, they are in fact, restricted to the developed European countries and do not cover the less-developed Middle- and East-European countries. Considerable progress can only be expected if

— people working on the problems of environment will have a wide overlook on the achievements and the existing information systems, and
— will co-ordinate their work and find new areas of environmental sciences to explore.

Beside the global and regional research, a wide international co-operation would considerably help the scientific investigations running now isolatedly in the countries or regions.

The aim of the EN-IN Conference is to provide a forum for the experts

involved in environmental research and informatics to exchange ideas, views, information and initiate a better co-operation.
Topics to be concerned are the followings:

Information systems of environmental management
- — environmental indicators, standards
- — local and regional information and their interrelations
- — networks of information systems.

Environmental monitoring systems
- — characterization of the environmental state and its changes
- — methodological tools for the evaluations of the environmental state and change.

Environmental modelling
- — simulation models
- — stochastic models
- — risk analysis
- — decision support system.

Environmental impact assessement
- — methodological tools and techniques
- — case studies.

Informatics in the environmental management
- — implementations of the information systems, software and hardware
- — geographical information systems
- — networks
- — managing of environmental hazards.

Deadlines for contributors. Submission of abstracts: January 31, 1995; proposal for invited sessions: January 31, 1995; notification of acceptance: March 15, 1995 and submission of full papers: May 15, 1995.

Two copies of abstracts (max. 200–300 words) in English should be sent to the Conference Secretariat, indicating the author(s) name, the title of the paper, the affiliation and the mailing address of the contact author.

Proposals for invited sessions must include a brief description of the topics and a list of prospective authors and titles.

Proceedings containing all accepted papers will be published and available for all registered participants.

An *exhibition* will be held during the Conference. Whoever is interested in exhibiting, please inform the Secretariat.

The Conference will take place at the *Hotel Agro* (H–1121 Budapest, Normafa út 54), situated on Szabadság Hill, a quiet, nice part of the capital, offering beautiful panoramas of the city. The Hotel has excellent conference facilities and can accommodate all participants at reasonable prices. Attractions include an indoor swimming pool and fitness centre; a scenic forest is close by.

Address of the Conference Secretariat:

EN + IN Conference
Viktor Richter
Computer and Automation Research Institute
H-1518 Budapest, P.O. Box 63, Hungary
Phone: +361 181 0511, 166-5644
Fax: +361 186 9378, 166-7503
E-mail: h8746 ric @ella.hu

Workshop on Regional Climatology
organized on the occasion of the 90th anniversary
of the Milešovka Observatory foundation

The workshop is organized by the Institute of Atmospheric Physics, and the National Committee for the National Climate Programme of the Czech Republic, under the auspices of the Czech Meteorological Society.

The workshop will be held on 11–15 September 1995 in Prague. One day excursion to the Milešovka Observatory is planned within the workshop.

It is intended to hold the following sessions:

— mountain climatology,
— climate variability,
— advanced methods in climatology,
— regional climate change scenarios,
— methods for assessing climate change impacts,
— adaptation and mitigation strategies.

If you intend to participate, please contact as soon as possible Dr. Ivana Nemešová at the following address:

Institute of Atmospheric Physics
Boční II 1401, 141 31 Praha 4, Czech Republic
Tel.: 42 2 769703
Fax: 42 2 763745

ATMOSPHERIC ENVIRONMENT

an international journal

To promote the distribution of Atmospheric Environment *Időjárás* publishes regularly the *contents* of this important journal. For further information the interested reader is asked to contact *Dr. P. Brimblecombe,* School for Environmental Sciences, University of East Anglia, Norwich NR 7TJ, U.K.

Volume 28 Number 14 1994

Volume 28 Number 15 1994

Short Communications

Volume 28 Number 16 1994

N. Dombrowski, E.A. Foumeny, D.B. Ingham and *Y.D. Qi*: Prediction of 'blowout' from deposition gauges, 2685-2690.

D.S. Lee, J.A. Garland and *A.A. Fox*: Atmospheric concentrations of trace elements in urban areas of the United Kingdom, 2691-2713.

L.A. Gundel, W.H. Benner and *A.D.A. Hansen*: Chemical composition of fog water and interstitial aerosol in Berkeley, California, 2715-2725.

R.C. Musselman, T. Younglove and *P.M. McCool*: Response of *Phaseolus vulgaris* L. to differing ozone regimes having identical total exposure, 2727-2731.

A. Eldering, G.R. Cass and *K.C. Moon*: An air monitoring network using continuous particles size distribution monitors: connecting pollutant properties to visibility via Mie scattering calculations, 2733-2749.

T.R. Quackenbush, M.E. Teske and *C.E. Polymeropoulos*: A model for assessing fuel jettisoning effects, 2751-2759.

Volume 28 Number 17 1994

J. Kukkonen, M. Kulmala, J. Nikmo, T. Vesala, D.M. Webber and *T. Wren*: The homogeneous equilibrium approximation in models of aerosol cloud dispersion, 2763-2776.

D.P. Chock, S.L. Winkler, T.Y. Chang, S.J. Rudy and *Z.K. Shen*: Urban ozone air quality impact of emissions from vehicles using reformulated gasolines and M85, 2777-2787.

L.A. Moy, R.R. Dickerson and *W.F. Ryan*: relationship between back trajectories and tropospheric trace gas concentrations in rural Virginia, 2789-2800.

A.E. Milionis and *T.D. Davis*: Regression and stochastic models for air pollution—I. Review, comments and suggestions, 2801-2810.

A.E. Milionis and *T.D. Davis*: Regression and stochastic models for air pollution—II. Application of stochastic models to examine the links between ground-level smoke concentrations and temperature inversions, 2811-2822.

N. Kumar, A.G. Russel, T.W. Tesche and *D.E. McNally*: Evaluation of CALGRID using two different ozone episodes and comparison to UAM results, 2823-2845.

O. Klemm and *E. Schaller*: Aircraft measurement of pollutant fluxes across the borders of Eastern Germany, 2847-2860.

R.F. Griffiths: Errors in the use of the Briggs parameterization for atmospheric dispersion coefficients, 2861-2865.

E. Ganor: The frequency of Saharan dust episodes over Tel Aviv, Israel, 2867-2871.

R. Chester, G.F. Bradshaw and *P.A. Corcoran*: Trace metal chemistry of the North Sea particulate aerosol; concentrations, sources and sea water fates, 2873-2883.

B. Telenta, N. Aleksic and *M. Dacic*: Application of the operational synoptic model for pollution forecasting in accidental situations, 2885-2891.

Volume 28 Number 18 1994

D.A. Westenbarger and *G.B. Frisvold*: Agricultural exposre to ozone and acid precipitation, 2895-2907.

A.C. Ward: A simple procedure for ranking the performance of several air-quality models across a number of different sites, 2909-2915.

H.W.M. Witlox: The HEGADAS model for ground-level heavy-gas dispersion—I. Steady-state model, 2917-2932.

H.W.M. Witlox: The HEGADAS model for ground-level heavy-gas dispersion—II. Time-dependent model, 2933-2946.

H.W.M. Witlox and *K. McFarlane*: Interfacing dispersion models in the HGSYSTEM hazard-assessment package, 2947-2962.

D.J. Hall, S.L. Upton and *G.W. Marsland*: Designs for a deposition gauge and a flux gauge for monitoring ambient dust, 2963-2979.

H.H. Suh, G.A. Allen, B. Aurian-Blăjeni, P. Koutrakis and *R.M. Burton*: Field method comparison for the characterization of acid aerosols and gases,2981-2989.

H.E. Jeffries and *S. Tonnesen*: A comparison of two photochemical reaction mechanisms using mass balance and process analysis, 2991-3003.

Xiaoming Zhang and *A.F. Ghoniem*: A computational model for the rise and dispersion of wind-blown, buoyancy-driven plumes—II. Linearly stratified atmosphere, 3005-3018.

Xiaoming Zhang and *A.F. Ghoniem*: A computational model for the rise and dispersion of wind-blown, buoyancy-driven plumes—III. Penetration of atmospheric inversion, 3019-3032.

J.W. Spence and *J.N. McHenry*: Development of regional corrosion maps for galvanized steel by linking the RADM engineering model with an atmospheric corrosion model, 3033-3046.

J.F. Hopper, D.E. Worthy, L.A. Barrie and *N.B.A. Trivett*: Atmospheric observations of aerosol black carbon, carbon dioxide, and methane in the high Arctic, 3047-3054.

Volume 28 Number 19 1994

B.J. Turpin, J.J. Huntzicker and *S.V. Hering*: Investigation of organic aerosol sampling artifacts in the Los Angeles basin, 3061-3071.

R.W. Simpson and *Hongchang Xu*: Atmospheric lead pollution in an urban area—Brisbane, Australia, 3073-3082.

V. Subramanyam, K.T. Valsaraj, L.J. Thibodeaux and *D.D. Reible*: Gas-to-particle partitioning of polycyclic aromatic hydrocarbons in an urban atmosphere, 3083-3091.

D.J. Moschandreas and *P.E. Chang*: On the use of a risk ladder: linking public perception of risks associated with indoor air with cognitive elements and attitudes toward risk reduction, 3093-3098.

D.J. Wilson and *B.K. Lamb*: Dispersion of exhaust gases from roof-level stacks and vents on a laboratory building, 3099-3111.

P. Goyal, M.P. Singh and *T.K. Bandyopadhyay*: Environmental studies of SO_2, SPM and NO_x over Agra, with various methods of treating calms, 3113-3123.

Yu-Mei Kuo and *Chih-Shan Li*: Seasonal fungus prevalance inside and outside of domestic environments in the subtropical climate, 3125-3130.

J.K. Mishra, R. Aarathi and *M.D. Joshi*: Remote sensing quantification and change detection of natural resources over Delhi, 3131-3137.

Chih-Shan Li: Elemental composition of residental indoor PM10 in the urban atmosphere of Taipei, 3139-3144.

L.T. Khemani, G.A. Momin, P.S.P. Rao, A.G. Pillai, P.D. Safai, K. Mohan and *M.G. Rao*: Atmospheric pollutants and their influence on acidification of rain water at an industrial location on the west coast of India, 3145-3154.

G. Lorenzini, C. Nali and *A. Panicucci*: Surface ozone in Pisa (Italy): a six-year study, 3155-3164.

O. Massambani and *F. Andrade*: Seasonal behavior of tropospheric ozone in the Sao Paulo (Brazil) Metropolitan Area, 3165-3169.

N. Mikac and *M. Branica*: Wet deposition of ionic alkylleads and total lead in urban areas of Croatia, 3171-3179.

J.G. Kretzschmar: Particulate matter levels and trends in Mexico City, Sao Paulo, Buenos Aires and Rio de Janeiro, 3181-3191.